

HOW ADVERSARIAL ATTACKS CAN DISRUPT SEEMINGLY STABLE ACCURATE CLASSIFIERS

OLIVER J. SUTTON¹, QINGHUA ZHOU¹, IVAN Y. TYUKIN¹, ALEXANDER N. GORBAN²,
ALEXANDER BASTOUNIS², AND DESMOND J. HIGHAM³

ABSTRACT. Adversarial attacks dramatically change the output of an otherwise accurate learning system using a seemingly inconsequential modification to a piece of input data. Paradoxically, empirical evidence indicates that even systems which are robust to large random perturbations of the input data remain susceptible to small, easily constructed, adversarial perturbations of their inputs. Here, we show that this may be seen as a fundamental feature of classifiers working with high dimensional input data. We introduce a simple generic and generalisable framework for which key behaviours observed in practical systems arise with high probability—notably the simultaneous susceptibility of the (otherwise accurate) model to easily constructed adversarial attacks, and robustness to random perturbations of the input data. We confirm that the same phenomena are directly observed in practical neural networks trained on standard image classification problems, where even large additive random noise fails to trigger the adversarial instability of the network. A surprising takeaway is that even small margins separating a classifier’s decision surface from training and testing data can hide adversarial susceptibility from being detected using randomly sampled perturbations. Counterintuitively, using additive noise during training or testing is therefore inefficient for eradicating or detecting adversarial examples, and more demanding adversarial training is required.

1. INTRODUCTION

Adversarial attacks aim to slightly modify a piece of input data in such a way as to significantly change the output of a model. As such, they exploit sensitivities and instabilities in neural networks. Recent work [2] has shown that such instabilities are somewhat inevitable, even in relatively small networks consisting of just two layers where the number of neurons is linear in the input data dimension. On top of this, there exist simple algorithms enabling a malicious attacker to produce adversarial perturbations quite easily in many cases [3]. It is remarkable, therefore, that these same instabilities are rarely triggered by random perturbations to the input data – even when these random perturbations may be much larger than destabilising adversarial perturbations.

This ‘paradox of apparent stability’ is demonstrated in Figure 1 for a standard convolutional neural network trained on CIFAR-10 images [11]. Although the majority of images in both the training and test data sets are susceptible to small adversarial attacks (Panel (a)), random perturbations even an order of magnitude larger mostly fail to cause the images to be misclassified (Panel (b)). These experiments are discussed in detail in Section 2.

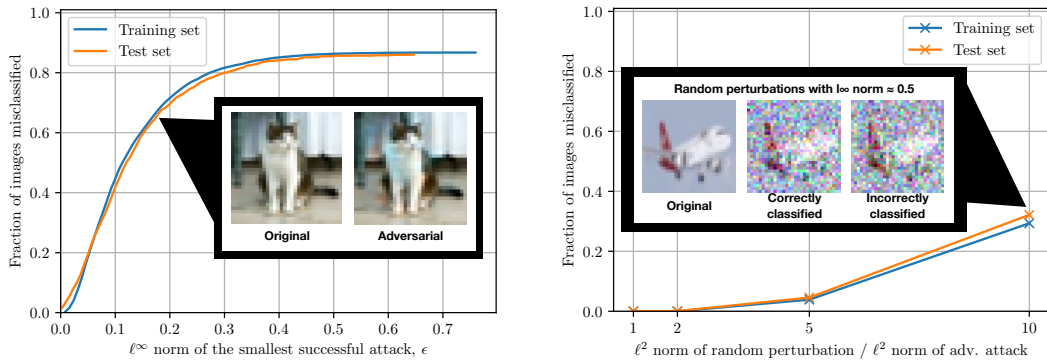
Several explanations for the causes of adversarial examples have been proposed in the literature. An early work on the subject [5] suggested that adversarial images simply live in regions of the data space to which the data distribution assigns low probability. A variant of this idea, discussed in [9], suggests that adversarial attacks perturb inputs in a way that moves them in an orthogonal direction to the local data manifold. This results in adversarial images which exist in a region of data space where no training data could have been sampled, and the decision surfaces of the network are therefore relatively pathological. Other suggested mechanisms include the dimpled manifold hypothesis [15], boundary tilting [18], and the existence of uncountably large families of special distributions for which instabilities are expected [2]. However, none of these frameworks

¹DEPARTMENT OF MATHEMATICS, KING’S COLLEGE LONDON, WC2R 2LS

²SCHOOL OF COMPUTING AND MATHEMATICAL SCIENCES, UNIVERSITY OF LEICESTER, LE1 7RH

³SCHOOL OF MATHEMATICS, UNIVERSITY OF EDINBURGH, EH9 3FD

E-mail addresses: oliver.sutton@kcl.ac.uk, qinghua.zhou@kcl.ac.uk, ivan.tyukin@kcl.ac.uk, a.n.gorban@leicester.ac.uk, ajb177@le.ac.uk, d.j.higham@ed.ac.uk.



(A) Cumulative histogram of sizes of successful adversarial attacks. (B) Sizes of successful random perturbations.

FIGURE 1. Histograms showing the fraction of images which were misclassified after either (a) an adversarial attack (as the fraction of ordinarily correctly classified images) or (b) a random perturbation of different sizes (as the fraction of images which were susceptible to adversarial attacks), measured as the maximum absolute change to an individual pixel channel (the ℓ^∞ norm). For adversarial attacks, this represents the smallest misclassifying attack in the adversarial direction, while for the random perturbations we record the smallest ℓ^∞ norm among all misclassifying perturbations. The random perturbations applied to each image were normalised to have Euclidean norm equal to a fixed multiple of the Euclidean norm of the smallest successful adversarial attack for that image, shown on the horizontal axis of panel (b). Examples are shown at the size of their respective perturbation norms.

rigorously account for and explain the paradoxical simultaneous robustness of these classifiers to random perturbations whose size could be several times larger than that of the adversarial ones.

Here, we suggest a resolution to the paradox rooted in ideas from the concentration effects of high dimensional probability distributions. We study the phenomenon in the context of a binary classification problem, and the simple, realistic framework we introduce captures the key features of the paradox which are observed in practice (precise definitions of these terms are given in Section 3):

Accuracy: The classifier correctly labels non-perturbed data.

Apparent stability: There is a vanishingly small probability that a sampled data point will be misclassified after a large random perturbation is applied to it.

Vulnerability: Yet, with high probability any sampled data point is susceptible to a very small adversarial perturbation that changes the predicted class.

Computability: The optimal destabilizing perturbation can be computed from knowledge of the loss function gradient.

A further important feature of the framework that we introduce is that it can easily be studied at various levels of generality, revealing that the phenomena we observe are not merely contrived artefacts. We first present the model in the case of two data distributions supported in n -dimensional balls with a linear classifier in Section 3. This simplified setting allows us to present results which distil the fundamental origins of the paradox without unnecessary technical details. We repeat the analysis in a general setting where data are sampled from two arbitrary distributions and a classifier with a nonlinear decision surface is deployed in Section E.

Our results reveal a tension between different notions of what it means for a classifier to be stable, a subtlety which is rarely discussed in practice. A problem may be *deterministically unstable* in the sense that there exists a small, destabilising perturbation, while the fact that this instability is extremely unlikely to be triggered by random noise in the data renders the problem

probabilistically stable. This is a dangerous situation for a performance-critical classifier: even though the performance appears excellent at test time, adversarial instabilities lurk awaiting an unscrupulous attacker and cannot be detected at random. We discuss this concept and further practical implications of our results in Section 4.

NOTATION

We use the following notation throughout:

- $x \cdot y$ denotes the inner product of $x, y \in \mathbb{R}^n$ and $\|x\| = \sqrt{x \cdot y}$ denotes the Euclidean norm,
- $\mathbb{B}_r^n(c) = \{x \in \mathbb{R}^n : \|x - c\| \leq r\}$ denotes the the Euclidean ball in \mathbb{R}^n with radius $r > 0$ centered at $c \in \mathbb{R}^n$, and we use the abbreviation $\mathbb{B}^n = \mathbb{B}_1^n(0)$,
- $V^n = \frac{\pi^{\frac{n}{2}}}{\Gamma(\frac{n}{2}+1)}$ denotes the n -dimensional volume of \mathbb{B}^n , and $V_{\text{cap}}^n(r, h)$ denotes the volume of the cap with height h of the n -dimensional ball of radius r , i.e. the volume of the set $\{x \in \mathbb{R}^n : \|x\| < r \text{ and } x_1 > 1 - h\}$, where $x_1 = x \cdot \mathbf{e}_1$ and $\mathbf{e}_1 = (1, 0, \dots, 0)^\top \in \mathbb{R}^n$.
- For a set $S \subset \mathbb{R}^n$, we use $\mathcal{U}(S)$ to denote the uniform distribution on S , and $\mathbb{I}_S : S \rightarrow \{0, 1\}$ to denote the indicator function of S , such that $\mathbb{I}_S(x) = 1$ for $x \in S$ and 0 otherwise.

2. THE PARADOX OF APPARENT STABILITY DEMONSTRATED ON CIFAR-10

The phenomenon of simultaneous susceptibility to adversarial attacks and robustness to random noise can be clearly demonstrated using the CIFAR-10 image classification dataset [11]. To present it in the simple setting of a binary classification problem, we split the 10 classes of the CIFAR-10 dataset into 45 binary classification problems. A separate network (each with an identical convolutional structure in the form of a truncated VGG network [16]) was trained using Tensorflow [1] for each of these problems, and each point in the training and test set was assessed for its susceptibility to adversarial examples using a gradient-based attack algorithm. On images which were susceptible to an adversarial attack with Euclidean norm δ , we applied 2000 randomly sampled perturbations with Euclidean norm ϵ which were set to be 1, 2, 5, and 10 times the size of δ to detect the sensitivity of the network to random perturbations around these images. The full experimental set up is described in Section A of the supplementary material.

The central phenomenon is illustrated in Figure 1: while the networks were easily fooled by relatively small adversarial perturbations which appear to make little perceptual difference to the image, they were remarkably robust to randomly sampled perturbations. Here we demonstrate this in the broadly representative case of the ‘aeroplane-vs-cat’ binary classification problem. Comparing the inset examples on Figures 1a and 1b, it is difficult to spot the modification made by the adversarial perturbation, and it is nearly equally difficult to make out the aeroplane in the randomly perturbed image. Note that, since the original images have pixel channel values in $[0, 1]$, a perturbation with ℓ^∞ norm greater than 1 represents a drastic change to the contents of the image, yet one which was rarely able to cause the network to misclassify its input. Further details of the experimental setup and full results for this and the remaining classification problems are explored in Section B of the supplementary material.

We also provide the results of experiments incorporating additive random noise to data at training time to assess the impact this may have on adversarial susceptibility (described in Sections A.4 and B.4). The conclusion we draw from these experiments is that training with even large random perturbations does not seem to significantly decrease the susceptibility to adversarial attacks, and is responsible for a large drop in accuracy.

3. AN ILLUSTRATIVE THEORETICAL MODEL

This puzzle can be understood via a simple yet reasonably generic model problem which captures the main features of the phenomenon. In this section, we focus on the case of two data distributions satisfying a mild non-degeneracy requirement (Definition 1) which are supported on balls and classified using a linear discriminant. A significantly more general version of this model is analysed in Section E of the supplementary material, with fewer constraints on the distributions and a classifier which is permitted to use a more general nonlinear decision surface. The results and

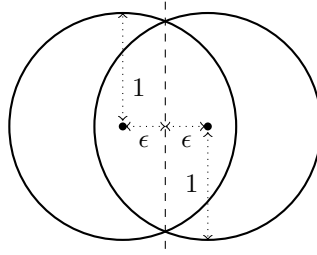


FIGURE 2. Two unit balls with centres separated by distance 2ϵ , and the decision surface of the classifier f (dashed).

conclusions remain largely qualitatively similar. In particular, the simultaneous co-existence of the high accuracy, the typicality of data susceptible to adversarial attacks, and the rarity of destabilising random perturbations with bounded ℓ^2 norm all extend to the more general model with nonlinear decision boundary (see Theorems 13, 15, 18 and Corollaries 14, 16, 19 in the Supplementary materials).

We recall the definition of a data distribution satisfying the Smearred Absolute Continuity (SmAC) property [6], which essentially just prevents it from having pathological concentration points. We note that if the growth property is satisfied with $A = 1$, then the distribution is simply the uniform distribution on the ball $\mathbb{B}_r^n(c)$.

Definition 1 (Smearred Absolute Continuity (SmAC) [6]). *A distribution \mathcal{D} on \mathcal{R}^n is said to satisfy the smearred absolute continuity condition if it possesses a density $p : \mathbb{R}^n \rightarrow \mathbb{R}_{\geq 0}$ and there exists a centre point $c \in \mathbb{R}^n$ and radius $r > 0$ such that $p(x) > 0$ only for points x in the ball $\mathbb{B}_r^n(c)$, and there exists a constant growth parameter $A > 0$ such that*

$$\sup_{x \in \mathbb{B}_r^n(c)} p(x) \leq \frac{A^n}{V^n r^n}.$$

Suppose that two classes of data are each sampled from data distributions \mathcal{D}_0 and \mathcal{D}_1 on \mathbb{R}^n satisfying the SmAC property. For simplicity, we suppose that these distributions each have radius 1 and centres given by $c_0 = -\epsilon \mathbf{e}_1$ and $c_1 = \epsilon \mathbf{e}_1$ respectively. We further suppose that both distributions satisfy the growth bound with the same parameter A . For brevity, we also define the combined distribution \mathcal{D}_ϵ which samples a point from \mathcal{D}_0 with label 0 with probability $\frac{1}{2}$, and samples a point from \mathcal{D}_1 with label 1 with probability $\frac{1}{2}$. The geometry of this setup is illustrated in Figure 2.

The classification function $f : \mathbb{R}^n \rightarrow \{0, 1\}$ with the highest accuracy which can be defined for this data model without further knowledge of the distributions is given by the simple linear separator

$$(1) \quad f(x) = \begin{cases} 0 & \text{if } x_1 < 0, \\ 1 & \text{otherwise.} \end{cases}$$

This classifier does not necessarily return the correct label in all cases since, for $\epsilon \in (0, 1)$, the two data classes overlap.

The first property of this simple model is that misclassified points are rare in the high dimensional setting, despite the fact that the two balls from which points are sampled have only a small separation between their centres. More precisely, the probability that this classifier is correct converges exponentially to 1 as the data dimension grows. This result is proven in Section C.1 of the supplementary material.

Theorem 2 (The classifier is accurate). *For any $\epsilon > 0$, the probability that the classifier applies the correct label to a randomly sampled data point grows exponentially to 1 with dimension n ,*

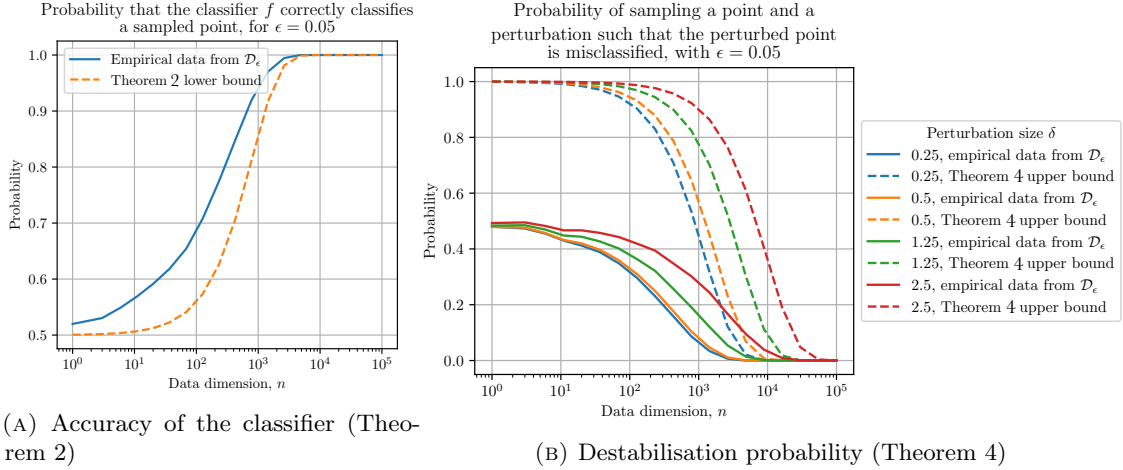


FIGURE 3. Comparison of the theoretical bounds in Theorems 2 and 4 against empirical results computed using 10,000 data points sampled from \mathcal{D}_ϵ , with $\epsilon = 0.05$, and 10,000 perturbations sampled from $\mathcal{U}(\mathbb{B}_\delta^n)$ for various values of δ . We see that, even for perturbations 50 times larger than the separation distance between the balls (i.e. $\delta = 2.5$), the probability of randomly sampling a perturbation which changes the classification of a random data point is very small in high dimensions.

specifically

$$P((x, \ell) \sim \mathcal{D}_\epsilon : f(x) = \ell) \geq 1 - \frac{1}{2}A^n(1 - \epsilon^2)^{\frac{n}{2}}.$$

The sharpness of this result is verified empirically in Figure 3a, computed for $A = 1$. We observe that by $n = 10,000$, the probability of sampling a point which will be misclassified is virtually 0. To put this and the following results into context, the $32 \times 32 \times 3$ images used in CIFAR-10 have 3,072 attributes, while the size of $256 \times 256 \times 3$ commonly used for the images in ImageNet have 196,608 attributes, placing them firmly within the range of dimensionalities where the effects described here are active.

On the other hand, even accurately classified points in this model are still close to the decision surface since the ball centres are only separated by distance ϵ . Because of this, for any $\delta > \epsilon$, there are points sampled from each class which are susceptible to an adversarial attack $s \in \mathbb{R}^n$ with $\|s\| \leq \delta$ which causes f to predict the wrong class. Moreover, in high dimensions, data points sampled from such a distribution concentrate at distance ϵ from this decision surface, meaning that the probability of sampling a point which is susceptible to an adversarial attack is high. This may be encapsulated in the following result, which is proven in Section C.2 of the supplementary material.

Theorem 3 (Susceptible data points are typical). *For any $\epsilon \geq 0$ and $\delta \in [\epsilon, 1 + \epsilon]$, the probability that a randomly sampled data point is susceptible to an adversarial attack with Euclidean norm δ grows exponentially to 1 with the dimension n , specifically*

$$\begin{aligned} P((x, \ell) \sim \mathcal{D}_\epsilon : \text{there exists } s \in \mathbb{B}_\delta^n \text{ such that } f(x + s) \neq \ell) \\ \geq 1 - \frac{1}{2}A^n(1 - (\delta - \epsilon)^2)^{\frac{n}{2}}. \end{aligned}$$

Although this susceptibility may therefore be viewed as typical in high dimensions, however, the probability of detecting it by sampling random perturbations of data points is paradoxically very small, as shown by the following result which is proven in Section C.3 of the supplementary material.

Theorem 4 (Destabilising perturbations are rare). *For any $\delta > \epsilon \geq 0$, the probability that a randomly selected perturbation with Euclidean norm δ causes a randomly sampled data point to be misclassified is bounded from above as:*

$$P((x, \ell) \sim \mathcal{D}_\epsilon, s \sim \mathcal{U}(\mathbb{B}_\delta^n) : f(x + s) \neq \ell) \leq A^n \left(1 - \left(\frac{\epsilon}{1 + \delta}\right)^2\right)^{\frac{n}{2}}.$$

In particular, when δ is independent of dimension n , this probability converges to 0 exponentially with n .

This probability bound is compared against empirically sampled data in Figure 3b. While the bound is not particularly sharp in low dimensions, it accurately describes the key phenomenon which is the convergence of the probability to 0 in high dimensions. This phenomenon is startlingly persistent, even when the magnitude of the sampled perturbations is 50 times greater than the distance between the centres of the spheres (when $\delta = 2.5$).

We note that some care needs to be taken when considering perturbations with fixed ℓ^∞ norms. The corresponding ℓ^2 norm of these perturbations scales as \sqrt{n} , affecting convergence to 0 of the probability of destabilisation (see Theorem 4).

A further aspect of this model problem is that successful adversarial attacks are universal in high dimensions. We define the *destabilisation margin* to be the distance by which a destabilising perturbation pushes a data point across the decision threshold of the classifier (1). This is measured by the functions $d_\ell : \mathbb{R}^n \times \mathbb{R}^n \rightarrow \mathbb{R}$ associated with each class $\ell = 0, 1$, where, for a data point x and a perturbation s ,

$$d_0(x, s) = \max\{x_1 + s_1, 0\},$$

and

$$d_1(x, s) = \max\{-x_1 - s_1, 0\}.$$

The following result then holds, as proven in Section C.4 of the supplementary material.

Theorem 5 (Universality of adversarial attacks). *Let $\epsilon \geq 0$ and suppose that $x, z \sim \mathcal{D}_\epsilon$ are independently sampled points with the same class label ℓ . For any $\gamma \in (0, 1]$, the probability that x is destabilised by all perturbations $s \in \mathbb{R}^n$ which destabilise z with destabilisation margin $d_\ell(z, s) > \gamma$ converges exponentially to 1 as the dimension n increases. Specifically, for $\ell \in \{0, 1\}$ and $z \in \mathbb{R}^n$, let $S_z = \{s \in \mathbb{R}^n : d_\ell(z, s) > \gamma\}$. Then,*

$$P(x, z \sim \mathcal{D}_\ell : f(x + s) \neq \ell \text{ for all } s \in S_z) \geq 1 - A^{2n} \left[1 - \left(1 - \frac{1}{2} \left(1 - \frac{\gamma^2}{4}\right)^{\frac{n}{2}}\right)^2\right].$$

The anatomy of this bound is slightly obfuscated at first glance by the presence of the distribution growth parameter A . In the case when $A = 1$, which implies that both distributions are uniform, the lower bound takes the simpler form $(1 - \frac{1}{2}(1 - \frac{\gamma^2}{4})^{\frac{n}{2}})^2$. When n is large, we may expect that the term $\frac{1}{2}(1 - \frac{\gamma^2}{4})^{\frac{n}{2}}$ is close to zero since $\gamma \in (0, 1]$, and the simplified bound is therefore close to 1. The value inside the square brackets of the general bound may therefore be expected to be close to 0, implying that the complete lower bound is close to 1 for sufficiently large n , even if A is large.

The dependence of the bound in Theorem 5 on the margin γ by which the perturbation destabilises z is an interesting feature. Roughly speaking, the result suggests that in low dimensions only severe perturbations which push points a long way past the decision threshold may be regarded as universal in the sense of having a high probability of destabilising other sampled points. As the dimension n increases, however, perturbations which produce smaller and smaller margins on individual points become universal in the sense that they have a constant probability of destabilising other sampled points.

Common algorithms for constructing adversarial attacks work by perturbing the target input in such a way as to increase an appropriate loss function. Gradient-based methods for this, such as the Fast Gradient Sign Method [5], compute the gradient of the loss function with respect to the components of the input, evaluated at the target input with its true class. Perturbing the input in the direction of this gradient therefore moves it in the direction of steepest ascent of the loss function locally, thereby representing a good candidate for an adversarial direction. The minimal

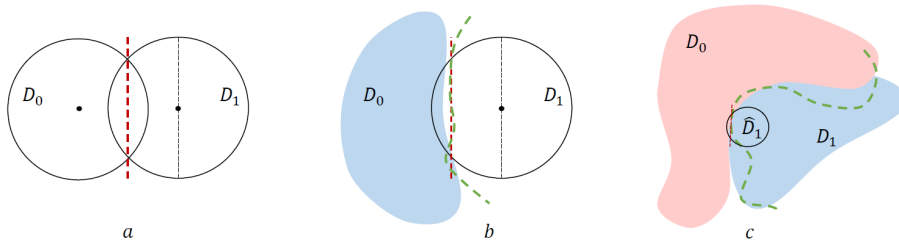


FIGURE 4. Different scenarios to which the simple two ball model may be generalised.

scaling to be applied to this adversarial direction, required to form the final adversarial input, can then be determined via a line search in the adversarial direction.

In the case of this model setup, such an algorithm (with a standard choice of loss function) will successfully provide the optimal direction for an adversarial attack: the most direct path to move the input along in order to cross the decision surface. To show this, we first observe that the classifier f in (1) can be equivalently defined as $f(x) = H(g(x))$, where $H : \mathbb{R} \rightarrow \{0, 1\}$ denotes the (piecewise constant) Heaviside function, and the linear function $g(x) = \mathbf{e}_1 \cdot x - \frac{1}{2}$. To construct gradient-based attacks, we use a differentiable version \tilde{f} of f constructed as $\tilde{f}(x) = \sigma(g(x))$, where $\sigma : \mathbb{R} \rightarrow (0, 1)$ is a continuously differentiable version of the Heaviside function which is monotonically increasing with $\sigma(0) = \frac{1}{2}$. An example of such a function is the standard sigmoid function. Then, the following result, proved in Section C.5 of the supplementary material, shows that gradient-based attacks on this classifier will always return the optimal attack direction.

Theorem 6 (Gradient-based methods find the optimal adversarial attack). *Let $L : \mathbb{R}_{>0} \rightarrow \mathbb{R}$ denote any differentiable, monotonically increasing loss function. For any $(x, \ell) \sim \mathcal{D}_\epsilon$, the gradient of the loss $L(|\tilde{f}(x) - \ell|)$ with respect to the components of x corresponds to a positive multiple of the optimal attack direction $(1 - 2\ell)\mathbf{e}_1$.*

3.1. Generalisations. Despite its simplicity, the model presented above covers a variety of settings, including data sampled from many common distributions such as uniform distributions and truncated Gaussian distributions. The model may also be directly generalised to cover an even wider range of settings. In Section E, we present analogous results for classifiers with non-flat decision surfaces separating two general distributions. As corollaries of these results, we obtain variants of the theorems presented above for the more general case when $r \neq 1$.

Further generalised scenarios in which our results may be applied are depicted in Figure 4. Panel *a* simply shows the original setup, with the red dashed line showing the decision surface of the classifier f .

Panel *b* visualises a more general case in which the data from only one class is supported in a ball and satisfies the SmAC property, while the other data class belongs to some different class of distributions. A more general non-flat decision boundary is depicted as a green dashed line in this case, which we suppose may be sufficiently well approximated *locally* by a hyperplane (depicted as a red dashed line). All results derived above (corresponding to the case of panel *a*) apply here for samples drawn from \mathcal{D}_1 .

Panel *c* shows the general setting in which both classes are sampled from non-SmAC distributions. However, if there is a subdomain \hat{D} near the decision surface within which one distribution is locally SmAC and the decision boundary in that domain is sufficiently well approximated locally by a hyperplane, then the problem can be considered as a local version of case *b*.

4. DISCUSSION AND RELATION TO PRIOR WORK

4.1. Existence of adversarial examples. Since the seminal work [17] reporting the discovery of adversarial examples in deep neural networks, the topic of adversarial examples as well as their origins and the mechanisms behind their occurrence have been the focus of significant attention in

theoretical and computational machine learning communities. One hypothesis, expressed in [17] was that the existence of the adversarial examples could be attributed to the inherent instabilities – i.e., large Jacobian norms leading to large Lipschitz constants for the classification maps. Theorems 3, 4 (see also Theorems 10 and 11 in Section D of the supplementary material) show that whilst the later mechanism may indeed constitute a feasible route for adversarial examples to occur, our presented framework reveals a simple and under-explored pathway for adversarial data to emerge naturally in systems without large Jacobian norms.

4.2. Fragility of adversarial examples. An interesting additional property of adversarial examples has been empirically observed in [12, 7]. It has been found that the capability of adversarial examples to fool the classifiers they have been designed for could be hindered by perturbations and transformations which are naturally present in real-world environments. Here we show and prove (Theorems 4 and 11) that in the vicinity of the target images, adversarial examples may indeed occupy sets whose Lebesgue measure is exponentially small. Hence, the addition of a small but appropriate perturbation to an example of that type will have the capability to make it non-adversarial.

4.3. Universality of adversarial examples. Another striking feature of adversarial examples is their potential universality. The phenomenon has first been reported in [13] and since then observed in a wide range of tasks and architectures [3]. Several explanations justifying the existence of universal adversarial examples have been proposed in the literature. This includes the view that universal perturbations may exploit correlated lower-dimensional structures in the classifier’s decision boundaries. It has been less clear how to explain the simultaneous existence, fragility, typicality, and universality of adversarial perturbations. Theorems 3, 4, and 5 show that the combination of these correlations with the high dimensionality of data may explain the co-existence of the typicality of adversarial examples, their fragility, and at the same time universality.

4.4. Typicality of adversarial examples. Several works have presented feasible mechanisms explaining the potential typicality and prevalence of adversarial data. In [14], [19] the authors exploited concentration of measure arguments to conclude that small destabilising perturbations can be typical in high dimensional settings. These arguments, however, do not explain the simultaneous rarity of destabilising random perturbations and the typicality of adversarial examples (see Fig. 6 and the discussion below). The connection of these two phenomena is a key feature of our framework.

4.5. Notions of stability. Our present work reveals a new unexplored relationship between stability and the existence of adversarial data. We show that the ubiquitous presence of adversarial data perturbations which destabilise the classifier is not contradictory to the robustness of the classifier to random perturbations of the data. If we view the former as a form of *deterministic instability* (i.e. there exist destabilising perturbations), and the latter as a form of *probabilistic stability* (destabilising perturbations are unlikely to be sampled at random), it becomes apparent that the probabilistic stability is in fact masking the underlying instability. Since these two notions of stability are clearly not equivalent, it is imperative to understand the distinctions between the two. To clarify this intriguing relationship, let us first recall two relevant definitions of stability (cf. [8]).

Definition 7 (ϵ -stability). *The classification map $f : \mathbb{R}^n \rightarrow \{0, 1\}$ is ϵ -stable at x if*

$$f(x + s) = f(x) \text{ for all } s \in \mathbb{B}_\epsilon^n.$$

Definition 8 (ϵ -stability with confidence v). *Let μ be a probability distribution on \mathbb{B}_ϵ^n . The classification map $f : \mathbb{R}^n \rightarrow \{0, 1\}$ is ϵ -stable at x with confidence v w.r.t. the distribution μ if*

$$P(s \sim \mu : f(x + s) = f(x)) \geq v.$$

At the core of the phenomenon explored in Theorems 3 and 4 is the fact that a “typical” point x is δ -stable with confidence v with respect to perturbations sampled from $\mathcal{U}(\mathbb{B}_\delta^n)$, where v approaches 1 exponentially in n . This makes the finding of adversarial perturbations by adding random samples $s \sim \mathcal{U}(\mathbb{B}_\delta^n)$ difficult and unlikely.

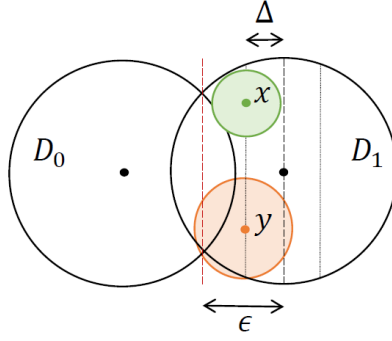


FIGURE 5. Adversarial susceptibility of seemingly stable classifiers. Points x and y are in the Δ thickening of disc intersecting the ball \mathcal{D}_1 along one of its largest equators. For n sufficiently large, most points sampled from $\mathcal{U}(\mathcal{D}_1)$ belong to this domain. Both x and y are $(\epsilon - \Delta)$ -stable. At the same time, they are also δ -stable with confidence $\nu \approx 1$.

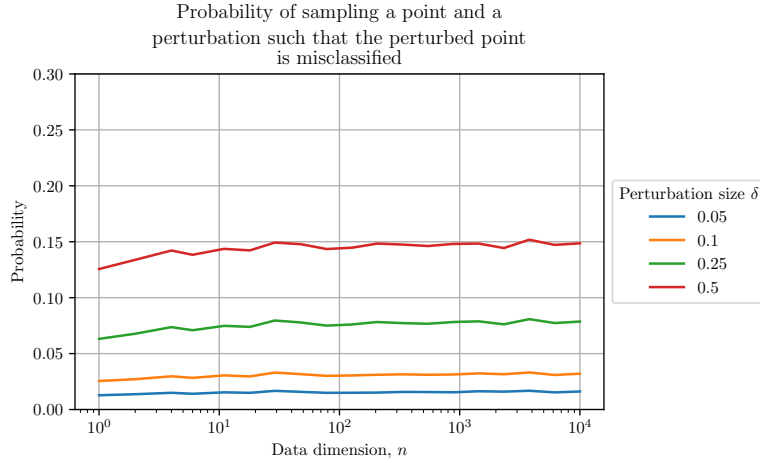


FIGURE 6. The empirical probability of sampling a point and perturbation of size δ such that the perturbed data point is misclassified, under the two hemispheres model with $\epsilon = 0$. This empirical data was computed by sampling 10,000 points from the hemisphere distribution and 10,000 perturbations from $\mathcal{U}(\mathbb{B}_\delta^n)$.

At the same time, for n sufficiently large, typical points are located in some $\Delta < \epsilon$ vicinity of the equators of the n -dimensional unit balls supporting \mathcal{D}_0 and \mathcal{D}_1 . This implies that these typical points are $\epsilon - \Delta$ -stable in the sense of Definition 7. This is visualised in the diagram shown in Figure 5. In the absence of the margin ϵ separating the centres of \mathcal{D}_0 and \mathcal{D}_1 , there is no room to “hide” adversarial examples among random perturbations. This leads to an intriguing observation:

The existence and prevalence of adversarial examples, which are undetectable via random perturbations, can sometimes be facilitated and even induced, by ϵ' -stability (for some appropriately chosen ϵ') of “typical” data samples.

To illustrate the practical consequences of this, we investigated a model in which two data classes were sampled from complementary half-balls separated by margin $\epsilon \geq 0$ (see Section D of the supplementary material). This choice of model is motivated by its ability to represent two separable classes without any margin or overlap. Figure 6 shows the results of numerical experiments computing the frequency with which sampled data was misclassified after random perturbations of the form $s \sim \mathcal{U}(\mathbb{B}_\delta^n)$ when $\epsilon = 0$, for different values of δ and n . This demonstrates

that in the absence of margins (which is an admissible case in the setup adopted in [14]) the probability of registering misclassifications due to random perturbation is significant and does not change much with dimension.

5. CONCLUSION

Our new framework for studying the paradox of apparent stability in classification problems allows for rigorous probabilistic bounds that are consistent with empirical observations concerning vulnerability to worst-case (Theorem 3), random (Theorem 4), universal (Theorem 5) and computable (Theorem 6) attacks. The results are generic in the sense that they deal with small perturbations under which any smooth and accurate classifier will behave like the optimal linear classifier (1). As illustrated in Figure 4 and Section 3.1, the setup can be generalised to cover a broad range of input distributions and classification boundaries. We envisage that the results will also extend readily to comparable multiclass problems. In addition to quantifying vulnerabilities, our analysis also raises new issues concerning the most relevant and useful notions of stability in classification.

The overlapping unit ball model that we used, and the two hemispheres model in Section D of the supplementary material, are closely tied to the use of the Euclidean norm. We note that there are several applications where spherical input data arises naturally, including remote sensing, climate change modeling, global ionospheric prediction and environmental governance, [4]. It would of course be of interest to establish the extent to which these results can be extended to other choices of norm and input domain. We also note that more customised results could be investigated for specific classification tools by exploiting further information, for example, about the architecture, training regime and level of floating point accuracy.

ACKNOWLEDGEMENTS

O.J.S., Q.Z., I.Y.T. and A.N.G. are grateful for financial support by the UKRI and EPSRC (UKRI Turing AI Fellowship ARaISE EP/V025295/1). I.Y.T. is also grateful for support from the UKRI Trustworthy Autonomous Systems Node in Verifiability EP/V026801/1. D.J.H. and A.B. were supported by EPSRC grant EP/V046527/1.

REFERENCES

- [1] M. Abadi, A. Agarwal, P. Barham, E. Brevdo, Z. Chen, C. Citro, G. S. Corrado, A. Davis, J. Dean, M. Devin, S. Ghemawat, I. Goodfellow, A. Harp, G. Irving, M. Isard, Y. Jia, R. Jozefowicz, L. Kaiser, M. Kudlur, J. Levenberg, D. Mané, R. Monga, S. Moore, D. Murray, C. Olah, M. Schuster, J. Shlens, B. Steiner, I. Sutskever, K. Talwar, P. Tucker, V. Vanhoucke, V. Vasudevan, F. Viégas, O. Vinyals, P. Warden, M. Wattenberg, M. Wicke, Y. Yu, and X. Zheng. TensorFlow: Large-scale machine learning on heterogeneous systems, 2015. URL <https://www.tensorflow.org/>. Software available from tensorflow.org.
- [2] A. Bastounis, A. C. Hansen, and V. Vlačić. The mathematics of adversarial attacks in AI—why deep learning is unstable despite the existence of stable neural networks. *arXiv preprint arXiv:2109.06098*, 2021.
- [3] A. Chaubey, N. Agrawal, K. Barnwal, K. K. Guliani, and P. Mehta. Universal adversarial perturbations: A survey. *arXiv preprint arXiv:2005.08087*, 2020.
- [4] H. Feng, S. Huang, and D.-X. Zhou. Generalization analysis of CNNs for classification on spheres. *IEEE Transactions on Neural Networks and Learning Systems*, pages 1–14, 2021. doi: 10.1109/TNNLS.2021.3134675.
- [5] I. J. Goodfellow, J. Shlens, and C. Szegedy. Explaining and harnessing adversarial examples. In Y. Bengio and Y. LeCun, editors, *3rd International Conference on Learning Representations, San Diego, CA*, 2015. URL <http://arxiv.org/abs/1412.6572>.
- [6] A. Gorban, A. Golubkov, B. Grechuk, E. Mirkes, and I. Tyukin. Correction of AI systems by linear discriminants: Probabilistic foundations. *Information Sciences*, 466: 303–322, 2018. ISSN 0020-0255. doi: <https://doi.org/10.1016/j.ins.2018.07.040>. URL <https://www.sciencedirect.com/science/article/pii/S0020025518305607>.

- [7] K. D. Gupta, D. Dasgupta, and Z. Akhtar. Applicability issues of evasion-based adversarial attacks and mitigation techniques. In *2020 IEEE Symposium Series on Computational Intelligence (SSCI)*, pages 1506–1515. IEEE, 2020.
- [8] P. Huang, Y. Yang, M. Liu, F. Jia, F. Ma, and J. Zhang. ϵ -weakened robustness of deep neural networks. In *Proceedings of the 31st ACM SIGSOFT International Symposium on Software Testing and Analysis*, pages 126–138, 2022.
- [9] M. Khoury and D. Hadfield-Menell. On the geometry of adversarial examples. *arXiv preprint arXiv:1811.00525*, 2018.
- [10] King’s College London. King’s Computational Research, Engineering and Technology Environment (CREATE), 2022. URL <https://doi.org/10.18742/rnvf-m076>.
- [11] A. Krizhevsky. Learning multiple layers of features from tiny images. Technical report, 2009.
- [12] A. Kurakin, I. J. Goodfellow, and S. Bengio. Adversarial examples in the physical world. In *Artificial intelligence safety and security*, pages 99–112. Chapman and Hall/CRC, 2018.
- [13] S.-M. Moosavi-Dezfooli, A. Fawzi, O. Fawzi, and P. Frossard. Universal adversarial perturbations. In *Proceedings of the IEEE conference on computer vision and pattern recognition*, pages 1765–1773, 2017.
- [14] A. Shafahi, W. Huang, C. Studer, S. Feizi, and T. Goldstein. Are adversarial examples inevitable? *International Conference on Learning Representations, New Orleans, USA*, 2019.
- [15] A. Shamir, O. Melamed, and O. BenShmuel. The dimpled manifold model of adversarial examples in machine learning. *arXiv preprint arXiv:2106.10151*, 2021.
- [16] K. Simonyan and A. Zisserman. Very deep convolutional networks for large-scale image recognition, 2015.
- [17] C. Szegedy, W. Zaremba, I. Sutskever, J. Bruna, D. Erhan, I. Goodfellow, and R. Fergus. Intriguing properties of neural networks. *arXiv preprint arXiv:1312.6199*, 2013.
- [18] T. Tanay and L. Griffin. A boundary tilting perspective on the phenomenon of adversarial examples. *arXiv preprint arXiv:1608.07690*, 2016.
- [19] I. Y. Tyukin, D. J. Higham, and A. N. Gorban. On adversarial examples and stealth attacks in artificial intelligence systems. In *2020 International Joint Conference on Neural Networks (IJCNN)*, pages 1–6. IEEE, 2020.

SUPPLEMENTARY MATERIAL

APPENDIX A. EXPERIMENTAL SETUP

To present the phenomenon in a simple setting, we arranged the 10 classes of the CIFAR-10 dataset into 45 binary classification problems.

A.1. Network architecture. Convolutional neural networks were trained on each of these problems, using the same architecture and training regime for each problem. In each case we used a simplification of the VGG architecture [16] adapted to the $32 \times 32 \times 3$ resolution of the CIFAR-10 images, the details of which are given in Table 1. The English names associated with each of the 10 classes are provided in Table 2.

For each pair-wise binary classification problem, the classes were assigned the labels 0 and 1, for compatibility with a standard sigmoid function on the output node of the network. A mean square error loss function was used to train the network in Tensorflow [1] using stochastic gradient descent for 100 epochs with Nesterov momentum parameter 0.9 and an initial learning rate of 0.1, which was halved every 20 epochs. Dropout was used on the convolutional layers during training, with a parameter of 0.4.

For the binary classification problem of distinguishing class i from class j , we denote the training set by $\mathcal{X}_{i,j}$, and the test set by $\mathcal{Y}_{i,j}$. The subsets of training and test images which were correctly classified by the network are then denoted by $\mathcal{X}_{i,j}^{\text{corr}} \subset \mathcal{X}_{i,j}$ and $\mathcal{Y}_{i,j}^{\text{corr}} \subset \mathcal{Y}_{i,j}$ respectively.

We are therefore able to compute the training and test accuracy of the network for the binary classification problem involving class i and class j as the percentages

$$(2) \quad 100 \frac{\text{card}(\mathcal{X}_{i,j}^{\text{corr}})}{\text{card}(\mathcal{X}_{i,j})} \quad \text{and} \quad 100 \frac{\text{card}(\mathcal{Y}_{i,j}^{\text{corr}})}{\text{card}(\mathcal{Y}_{i,j})},$$

respectively, where we use card to denote the cardinality of a set.

A.2. Adversarial attacks. To investigate the susceptibility of the networks to adversarial attacks, we used a standard gradient-based algorithm on a loss function, which can be viewed as an Euclidean version of the Fast Gradient Sign Method (FGSM) introduced in [5]. Specifically, if $L(x, y, N)$ denotes the mean square error loss function evaluated on the neural network N at the

Layer	Size	Output channels	Number of trainable parameters
Conv-1	3×3	64	1,792
Conv-2	3×3	64	36,928
Max pooling	2×2		
Conv-3	3×3	128	73,856
Conv-4	3×3	128	147,584
Max pooling	2×2		
Conv-5	3×3	256	295,168
Conv-6	3×3	256	590,080
Dense		512	131,584
Dense		1	513

TABLE 1. Architecture used for the CIFAR-10 binary classification problems. All convolutional layers do not pad their output, meaning that the output shape of Conv-6 is $1 \times 1 \times 256$, and are followed by a leaky ReLU activation function with leakiness parameter 0.1. The final dense layer has a standard sigmoid activation function.

Index	Name
0	Aeroplane
1	Automobile
2	Bird
3	Cat
4	Deer
5	Dog
6	Frog
7	Horse
8	Ship
9	Truck

TABLE 2. Class names associated with each class index.

target image x with label ℓ , we compute the adversarial attack direction as

$$a(x) = \frac{\nabla_x L(x, \ell, N)}{\|\nabla_x L(x, \ell, N)\|},$$

where $\|\cdot\|$ denotes the Euclidean norm. We then tested 100 equally-spaced scalings $\epsilon \in [0, 5]$ to determine the smallest value such that $|\ell - N(x + \epsilon a(x))| > \frac{1}{2}$. This value of ϵ therefore gives the Euclidean norm of the smallest perturbation (among those tested) in the direction of $a(x)$ such that the network therefore predicts the wrong class for the attacked image. The value of ϵ therefore provides an upper bound on the minimal Euclidean distance of the image x from the decision surface of the neural network N .

For the class i vs class j binary classification problem, we use $\mathcal{X}_{i,j}^{\text{adv}} \subset \mathcal{X}_{i,j}^{\text{corr}}$ to denote the set of training images $x \in \mathcal{X}_{i,j}^{\text{corr}}$ such that x was correctly classified by the network, but $x + \epsilon a(x)$ was misclassified for at least one of our tested values of ϵ . The equivalent subset of the test set is denoted by $\mathcal{Y}_{i,j}^{\text{adv}} \subset \mathcal{Y}_{i,j}^{\text{corr}}$. We may then define the *adversarial susceptibility* of the network for the training and test sets as the percentages

$$(3) \quad 100 \frac{\text{card}(\mathcal{X}_{i,j}^{\text{adv}})}{\text{card}(\mathcal{X}_{i,j}^{\text{corr}})}, \text{ and } 100 \frac{\text{card}(\mathcal{Y}_{i,j}^{\text{adv}})}{\text{card}(\mathcal{Y}_{i,j}^{\text{corr}})},$$

respectively, where we use card to denote the cardinality of a set.

The results of these experiments are reported in Section B.2.

A.3. Random perturbations. To assess the effect on the network of random perturbations to the images, we sampled a set P of 2000 random perturbations from a uniform distribution on the d -dimensional ball with Euclidean norm ≤ 1 , where $d = 3,072$ denotes the number of individual attributes of a $32 \times 32 \times 3$ CIFAR-10 image. Then, for each pair i, j of classes, we performed the following experiment. For each image x in the subsets $\mathcal{X}_{i,j}^{\text{adv}}$ and $\mathcal{Y}_{i,j}^{\text{adv}}$ of the training and test sets which were susceptible to an adversarial attack, we constructed the perturbed image $x + \delta \epsilon s$ for each $s \in P$, where ϵ denotes the Euclidean norm of the smallest successful adversarial attack on x , scaled by each value of $\delta \in \{1, 2, 5, 10\}$ sequentially. In other words, we evaluated the network on an image which was perturbed by a random perturbation with Euclidean norm scaled by a fixed multiple of that of the (known successful) adversarial attack.

For the class i vs class j binary classification problem, we define the set $\mathcal{X}_{i,j}^{\text{rand},\delta} \subset \mathcal{X}_{i,j}^{\text{adv}}$ as the set of images which were susceptible to one or more random perturbations with scaling factor δ , as described above. The set $\mathcal{Y}_{i,j}^{\text{rand},\delta} \subset \mathcal{Y}_{i,j}^{\text{adv}}$ is defined analogously on the test set of images.

This enables us to define the *random perturbation susceptibility* of each network for the training and test sets as the percentages

$$(4) \quad 100 \frac{\text{card}(\mathcal{X}_{i,j}^{\text{rand},\delta})}{\text{card}(\mathcal{X}_{i,j}^{\text{adv}})}, \text{ and } 100 \frac{\text{card}(\mathcal{Y}_{i,j}^{\text{rand},\delta})}{\text{card}(\mathcal{Y}_{i,j}^{\text{adv}})},$$

respectively for each tested value of δ , where we use card to denote the cardinality of a set.

	1	2	3	4	5	6	7	8	9
0	99.88, 96.45	99.31, 91.70	99.40, 95.20	99.36, 94.65	99.67, 95.45	99.25, 96.05	99.49, 96.45	99.73, 94.10	99.77, 95.40
1		99.67, 96.65	99.46, 95.95	99.78, 98.10	99.75, 97.55	99.17, 96.85	99.91, 98.80	99.72, 96.85	99.77, 93.65
2			99.08, 85.20	99.70, 87.25	99.35, 87.05	99.68, 91.05	99.63, 92.90	99.58, 95.30	99.42, 95.80
3				98.74, 86.70	99.77, 82.60	99.09, 88.80	99.68, 91.35	99.53, 96.05	99.47, 95.05
4					99.59, 90.60	99.84, 94.90	99.78, 90.30	99.58, 97.20	99.42, 96.75
5						99.79, 93.95	99.72, 90.40	99.60, 96.85	99.41, 96.05
6							99.85, 96.70	99.40, 97.10	99.72, 97.20
7								99.70, 97.65	99.85, 97.60
8									99.78, 95.80

TABLE 3. Accuracy of the networks on the binary classification problems, reported in the form ‘train accuracy, test accuracy’, where accuracy is calculated as the percentage of images which were correctly classified. The row and column headers indicate the classes used in each binary classification problem.

The results of these experiments are reported in Section B.3.

A.4. Training with random perturbations. We explored the effect of applying additive random noise to images during training on adversarial robustness. To do this we inserted a layer at the beginning of the network architecture described in Table 1 which sampled noise from a prescribed distribution independently for each input and added it to the input. The precise random perturbation added to each image is therefore different each time the image is presented to the network during training. The random perturbation layer is only active during training, so does not affect how the trained network is assessed at test time. We experimented with noise sampled uniformly from the cube $[-a, a]^n$ (i.e. with maximum ℓ^∞ norm $a > 0$ and with noise sampled from the ball \mathbb{B}_b^n (i.e. with maximum Euclidean norm $b > 0$), with $a \in \{0.1, 0.5, 1.0\}$, $b \in \{3.2, 16, 32\}$, where $n = 32 \times 32 \times 3 = 3072$ is the dimension of a CIFAR-10 image. These values of a and b were selected to ensure that for each pair of a and b values the samples from each distribution would have approximately the same Euclidean norm on average. This enables us to observe whether the sampling distribution makes a significant impact on the results, independently of the magnitude. Each network was otherwise trained exactly as described in Section A.1. We report the results of these experiments in Section B.4.

APPENDIX B. DISCUSSION OF EXPERIMENTAL RESULTS

We now discuss the results of the experiments outlined in Section A. These results were computed using the CREATE HPC facilities at King’s College London [10].

B.1. Network performance. The training and test accuracy of the networks trained on each of the binary classification problems is shown in Table 3. The mean accuracy on the training set of the networks trained for all of the binary classification problems was 99.57% (standard deviation 0.24), with a minimum of 98.74%. In comparison, the mean accuracy on the test set was 94.09% (standard deviation 3.78), with a minimum of 82.6%. These figures indicate that the networks were generally quite capable to learning these binary classification problems, despite the fact they were trained using the same regime for only 100 training epochs each, and no specific tweaks were applied to improve the performance of any network.

B.2. Adversarial attacks. We report the adversarial susceptibility of each network (as defined in Section A.2) in Table 4. On average over all the binary classification problems, 85.0% of the training images were susceptible to an adversarial attack (standard deviation 9.71) with a minimum of 70.28%, while the average on the test set was 79.48% (standard deviation 7.91) with a minimum of 69.82%. We note that both minima were attained on the same task ‘frog-vs-ship’ (6-vs-8). In the vast majority of the binary classification problems, over 80% of images in the training and test sets could be adversarially attacked in such a way that they would be misclassified by the network. This demonstrates the susceptibility of all of the networks to adversarial attacks, implying that the decision surface in each case passes close to most of the points in the training and test sets.

	1	2	3	4	5	6	7	8	9
0	88.33, 86.88	95.69, 96.24	86.74, 86.08	95.19, 94.35	85.27, 83.97	83.43, 81.68	89.47, 88.02	92.78, 91.87	74.23, 73.69
1		86.25, 86.08	84.52, 83.79	93.59, 92.92	89.94, 88.83	85.23, 85.91	97.17, 97.17	89.62, 88.80	87.85, 88.04
2			91.88, 89.96	99.54, 99.66	96.93, 96.50	96.75, 96.05	92.97, 93.16	85.14, 83.89	92.73, 92.75
3				93.85, 92.85	99.86, 99.82	98.49, 98.65	98.95, 98.63	91.93, 92.04	78.84, 78.12
4					98.97, 98.34	98.99, 98.79	99.77, 99.56	80.96, 80.45	90.02, 90.08
5						96.19, 95.48	99.61, 99.61	84.14, 83.32	72.53, 71.63
6							98.63, 98.76	70.28, 69.82	87.35, 88.22
7								82.60, 83.56	96.85, 96.82
8									79.41, 78.03

TABLE 4. Susceptibility of the networks to adversarial attacks, reported in the form ‘train susceptibility, test susceptibility’, where susceptibility is calculated as in (3) as the percentage of images from the training set and test set which were misclassified after an adversarial attack using the algorithm described in Section A.2. The row and column headers indicate the classes used in each binary classification problem.

To measure just how close the decision surface passes to each data point, we also explore the sizes of the computed adversarial perturbations measured in several norms. In Table 5 we show the mean and standard deviations over each training and test set of the Euclidean norms of the smallest computed adversarial attack on each image. Similarly, Table 6 shows the mean and standard deviations over each training and test set of the ℓ^1 norms of the adversarial attacks, while Table 7 shows the same information for the ℓ^∞ norms.

The summary statistics reported in these tables are broken down in violin plots for a representative sample of the binary classification problems (selected, for simplicity, as the ‘ i -vs- $(i+1)$ ’ problems). These show an approximation of the distribution of the Euclidean norms (Figure 7), ℓ^∞ norms (Figure 8) and ℓ^1 norms (Figure 9) of adversarial attacks. In each case, this is the distribution across the whole training or test set of the norm of the smallest misclassifying adversarial attack found for each image using the algorithm described in Section A.2. It is clear from these plots that for the majority of the adversarial attacks the largest change to any individual pixel value is comparatively small: the ℓ^∞ norm is less than 0.2 for most of the images across all tasks. The ℓ^1 norms, on the other hand, compute the sum of the absolute value of all changes to all pixels, so are expected to be a much larger value. Scaling these ℓ^1 norms by the number of pixel channels ($32 \times 32 \times 3 = 3,072$), we obtain the mean absolute change to a single pixel. Taking 100 as a representative maximum value for the ℓ^1 norm across the majority of cases, we can therefore observe that this would correspond to a mean absolute change of approximately 0.03. Comparing this value to a similarly representative value of less than 0.5 for the ℓ^∞ norm of the adversarial attack, it is clear that this implies that the attacks are typically very localised since most of the change must be focused in just a few pixels.

The plots also indicate that the networks trained on certain tasks (such as ‘bird-vs-cat’ (2-vs-3) and ‘cat-vs-deer’ (3-vs-4) seem to be much more susceptible to small adversarial attacks. We mean this in the sense that while the overall attack susceptibility (Table 4) is quite typical, the attacks themselves on these classes appear to have much smaller norms.

The conclusion from these experiments is that most points in all of the training and test sets lie very close to the decision surface of the neural network, implying that the networks are susceptible to small perturbations to most of their training and test data.

B.3. Random perturbations. To explore whether the sensitivities discovered in Section B.2 could be triggered by random perturbations to the input data, we used the approach outlined in Section A.3. We report the random perturbation susceptibility of each network (as defined in Section A.3) in Table 8 for $\delta = 1$, Table 9 for $\delta = 2$, Table 10 for $\delta = 5$, and Table 11 for $\delta = 10$.

The remarkable story shown by this data is that the networks are almost universally insensitive to random perturbations to the images, even when those perturbations become quite drastic. This puzzling feature is demonstrated in Figures 10 and 11, where we show examples from the ‘aeroplane-vs-cat’ binary classification problem (0-vs-3), of images of a cat and an aeroplane

	1	2	3	4	5	6	7	8	9
0 train	1.25 (0.92)	0.76 (0.60)	1.19 (0.86)	0.96 (0.84)	1.32 (0.94)	1.21 (0.83)	1.24 (0.92)	0.84 (0.81)	1.20 (1.01)
test	1.25 (0.94)	0.79 (0.66)	1.21 (0.92)	0.97 (0.81)	1.36 (0.97)	1.24 (0.83)	1.26 (0.94)	0.83 (0.83)	1.25 (1.03)
1 train		1.32 (0.93)	1.00 (0.58)	1.13 (0.82)	1.27 (0.71)	0.96 (0.63)	1.50 (0.92)	1.08 (0.86)	0.75 (0.74)
test		1.35 (0.96)	1.00 (0.58)	1.14 (0.86)	1.28 (0.70)	0.99 (0.62)	1.47 (0.91)	1.06 (0.87)	0.74 (0.75)
2 train			0.40 (0.31)	0.48 (0.37)	0.64 (0.53)	0.56 (0.45)	0.86 (0.70)	1.05 (0.72)	1.21 (0.89)
test			0.37 (0.32)	0.47 (0.41)	0.63 (0.58)	0.57 (0.51)	0.86 (0.75)	1.06 (0.75)	1.22 (0.90)
3 train				0.47 (0.41)	0.40 (0.26)	0.74 (0.55)	0.58 (0.45)	1.27 (0.87)	0.72 (0.45)
test				0.44 (0.40)	0.35 (0.31)	0.73 (0.58)	0.57 (0.46)	1.29 (0.89)	0.72 (0.46)
4 train					0.68 (0.50)	0.54 (0.40)	0.65 (0.44)	1.17 (0.90)	1.03 (0.75)
test					0.67 (0.53)	0.53 (0.43)	0.63 (0.50)	1.21 (0.91)	1.07 (0.76)
5 train						0.75 (0.58)	0.73 (0.50)	1.33 (0.90)	0.94 (0.68)
test						0.77 (0.59)	0.70 (0.53)	1.32 (0.90)	0.98 (0.71)
6 train							0.82 (0.49)	1.38 (1.06)	0.94 (0.56)
test							0.83 (0.51)	1.42 (1.08)	0.97 (0.58)
7 train								1.39 (0.93)	1.05 (0.69)
test								1.41 (0.97)	1.05 (0.66)
8 train									1.14 (1.02)
test									1.13 (1.05)

TABLE 5. Means and standard deviations of the Euclidean norms of the smallest successful adversarial attack on each image in the training and test set, reported in the form ‘mean (standard deviation)’. The numbers in the row and column headers indicate the classes used in each binary classification problem. The ‘train’ row shows the values computed over the training set, while the ‘test’ row shows the values computed over the test set.

	1	2	3	4	5	6	7	8	9
0 train	43.58 (31.63)	24.81 (19.52)	40.77 (30.04)	32.93 (29.12)	43.40 (31.07)	40.08 (27.55)	43.21 (32.21)	27.75 (26.27)	41.17 (34.03)
test	43.75 (32.53)	25.80 (21.35)	41.29 (31.76)	33.23 (28.07)	44.58 (31.90)	41.01 (27.42)	43.99 (32.61)	27.31 (26.69)	42.73 (35.09)
1 train		43.67 (30.41)	31.26 (18.66)	37.92 (26.88)	41.80 (23.68)	30.91 (20.83)	50.20 (30.37)	36.27 (28.58)	23.48 (22.71)
test		44.62 (31.28)	31.42 (18.83)	38.38 (28.13)	42.21 (23.44)	31.85 (20.46)	49.17 (29.95)	35.49 (28.86)	23.24 (23.52)
2 train			13.21 (10.15)	15.77 (12.02)	20.75 (17.32)	18.44 (14.49)	28.16 (23.22)	34.41 (23.75)	39.90 (29.16)
test			12.27 (10.59)	15.37 (13.53)	20.27 (18.76)	19.03 (16.61)	28.24 (24.51)	34.76 (24.91)	40.46 (29.26)
3 train				15.75 (13.50)	12.88 (8.26)	23.30 (17.50)	19.21 (14.39)	43.05 (29.57)	23.97 (15.48)
test				14.86 (13.22)	11.22 (9.67)	23.05 (18.58)	18.90 (15.04)	43.74 (30.26)	24.07 (15.69)
4 train					23.18 (17.02)	18.52 (13.60)	19.96 (13.64)	38.80 (30.40)	33.26 (23.93)
test					22.81 (18.14)	18.22 (14.59)	19.39 (15.33)	40.01 (30.97)	34.66 (24.06)
5 train						23.89 (18.77)	23.76 (15.43)	45.22 (30.63)	30.60 (22.05)
test						24.53 (19.03)	22.78 (16.78)	45.22 (30.79)	31.86 (23.00)
6 train							27.77 (16.80)	46.02 (35.74)	30.55 (18.78)
test							27.97 (17.57)	47.44 (36.49)	31.66 (19.39)
7 train								47.05 (31.64)	35.33 (22.86)
test								47.78 (33.38)	35.27 (22.17)
8 train									38.53 (34.28)
test									38.29 (35.17)

TABLE 6. Means and standard deviations of the ℓ^1 norms of the successful adversarial attacks on each training and test set, reported in the form ‘mean (standard deviation)’. The numbers in the row and column headers indicate the classes used in each binary classification problem. The ‘train’ row shows the values computed over the training set, while the ‘test’ row shows the values computed over the test set.

	1	2	3	4	5	6	7	8	9
0 train	0.14 (0.11)	0.09 (0.08)	0.13 (0.09)	0.11 (0.10)	0.16 (0.12)	0.14 (0.10)	0.14 (0.11)	0.10 (0.10)	0.14 (0.12)
0 test	0.14 (0.11)	0.10 (0.09)	0.13 (0.10)	0.12 (0.10)	0.17 (0.13)	0.14 (0.10)	0.15 (0.12)	0.10 (0.10)	0.14 (0.12)
1 train		0.16 (0.12)	0.13 (0.08)	0.13 (0.10)	0.15 (0.09)	0.11 (0.07)	0.18 (0.12)	0.13 (0.11)	0.10 (0.10)
1 test		0.16 (0.13)	0.13 (0.08)	0.13 (0.11)	0.16 (0.09)	0.11 (0.07)	0.18 (0.12)	0.13 (0.11)	0.09 (0.10)
2 train			0.05 (0.04)	0.06 (0.04)	0.08 (0.07)	0.07 (0.06)	0.11 (0.10)	0.13 (0.09)	0.15 (0.12)
2 test			0.04 (0.04)	0.05 (0.05)	0.08 (0.07)	0.07 (0.06)	0.11 (0.11)	0.13 (0.10)	0.15 (0.12)
3 train				0.05 (0.05)	0.06 (0.04)	0.10 (0.07)	0.08 (0.06)	0.15 (0.11)	0.09 (0.06)
3 test				0.05 (0.05)	0.05 (0.05)	0.10 (0.08)	0.07 (0.07)	0.15 (0.11)	0.09 (0.06)
4 train					0.08 (0.06)	0.06 (0.05)	0.09 (0.07)	0.15 (0.11)	0.13 (0.10)
4 test					0.07 (0.06)	0.06 (0.06)	0.09 (0.07)	0.15 (0.11)	0.13 (0.10)
5 train						0.10 (0.08)	0.10 (0.08)	0.15 (0.11)	0.12 (0.09)
5 test						0.10 (0.08)	0.10 (0.08)	0.15 (0.11)	0.12 (0.10)
6 train							0.10 (0.06)	0.17 (0.13)	0.11 (0.07)
6 test							0.10 (0.06)	0.17 (0.14)	0.12 (0.07)
7 train								0.16 (0.11)	0.13 (0.09)
7 test								0.16 (0.12)	0.13 (0.08)
8 train									0.15 (0.14)
8 test									0.15 (0.15)

TABLE 7. Means and standard deviations of the ℓ^∞ norms of the smallest successful adversarial attack on each image in the training and test set, reported in the form ‘mean (standard deviation)’. The numbers in the row and column headers indicate the classes used in each binary classification problem. The ‘train’ row shows the values computed over the training set, while the ‘test’ row shows the values computed over the test set.

(original image in panel (a)) which were correctly classified by the network, alongside the same image after an adversarial attack which successfully changed the network’s predicted class in panel (b). This adversarial attack makes only a small change to the image (the largest change to any single pixel channel is 0.19 for the cat and 0.05 for the aeroplane). When the image is perturbed using a large random perturbation, as shown in panel (c), however, the network still produces the correct classification. For comparison, in panel (d) we show a random perturbation which caused the network to misclassify the image. Both of these random perturbations were obtained using $\delta = 10$ as in Section A.3 and therefore have similar norms. To the human eye, however, there is no significant difference between the two randomly perturbed images, or between the original image and the adversarially attacked image. Even in these cases where a random perturbation was found which caused a misclassification, it is to be noted that only a small fraction of the 2,000 sampled random perturbations did so (0.0415% for the cat and 0.002% for the aeroplane).

The data from Tables 8–11 shows that as the scale of the random perturbations increases (as controlled by δ), so too does the probability of causing a perturbed image to be misclassified. In itself, this observation is unsurprising, but the data in Table 10 shows that, even when the random perturbations are scaled to be 5 times larger than the known adversarial attack (measured in the Euclidean norm, corresponding to $\delta = 5$), typically fewer than 5% of images were misclassified after applying any of the random perturbations.

In Figures 12–14 we show the distributions of the smallest random perturbation found to cause an image to be misclassified, as measured in the Euclidean, ℓ^∞ and ℓ^1 norms respectively, for $\delta = 10$ on a representative sample of the binary classification problems (the ‘ i -vs- $(i + 1)$ ’ problems, as studied in Section B.2, cf. Figures 7–9). Recall that the random perturbations were sampled from a ball with Euclidean norm less than or equal to 1 (although high dimensional concentration phenomena ensure that the all of the random perturbations have Euclidean norm very close to 1), and were scaled by δ times the Euclidean norm of the smallest successful adversarial attack when used to attack each image. This explains the underlying similarity between these distributions and those in Figures 7–9, which show the size distributions of the adversarial attacks. However, it is readily

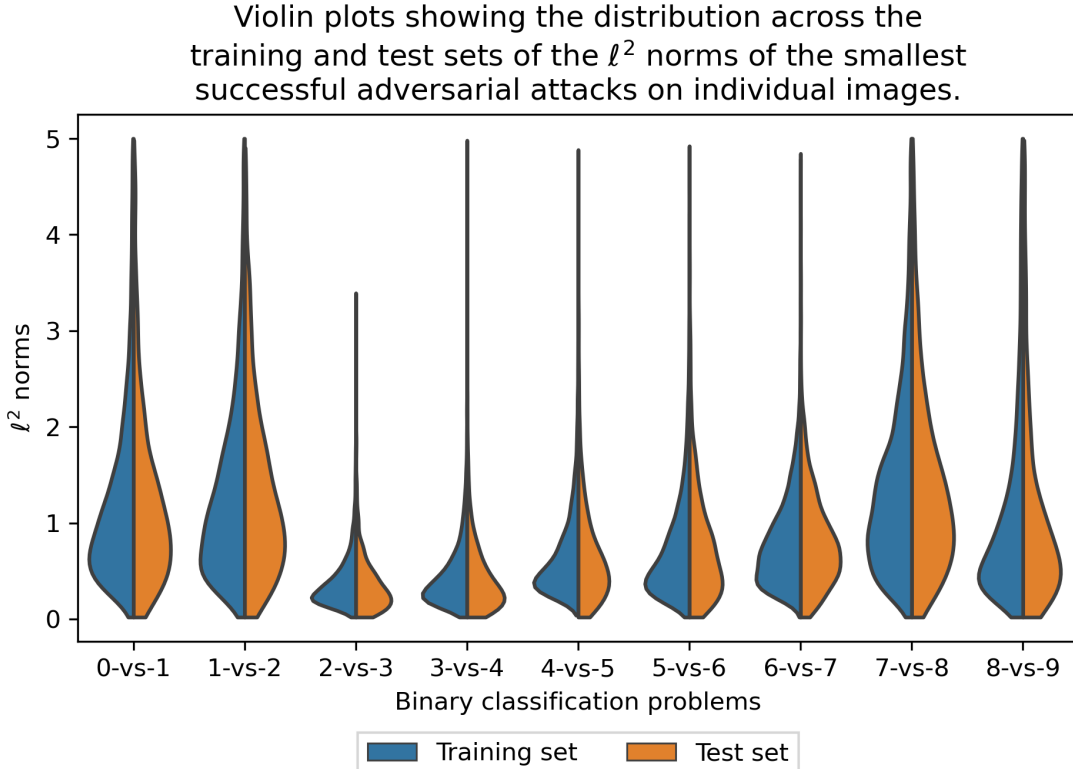


FIGURE 7. The distribution of the Euclidean norms of the successful adversarial attacks found for each image using the algorithm in Section A.2, shown for a representative sample of the binary classification problems. The plotted distributions were fitted to the data using a standard Kernel Density Estimation algorithm and therefore only provide an approximation of the true empirical distribution.

apparent here once again that significantly larger random perturbations are required as compared to adversarial perturbations. This is visible (and shown in more detail for the ‘cat-vs-aeroplane’ problem (0-vs-3) in Figure 15 from the fact that the random perturbation distributions appear to have much thicker tails than those for the adversarial perturbations; if simply a fixed fraction of all random perturbations were successful in causing an image to be misclassified then the distributions would shrink by a constant factor along their length.

Together, this evidence indicates that the decision surface does not pass close to the image in all directions, but rather only in one or a few specific adversarial directions.

B.4. Training with random perturbations. For brevity, we only report the results of these experiments for the representative subset of ‘class i -vs-class $i + 1$ ’ binary classification problems. These are given in Tables 12, 14 and 16 for random perturbations sampled uniformly from the cube $[-a, a]^n$ with $a \in \{0.1, 0.5, 1.0\}$ respectively, and Tables 13, 15 and 17 for noise sampled uniformly from the ball \mathbb{B}_b^n with $b \in \{3.2, 16, 32\}$ respectively (see Section A.4 for details of the experimental setup). These results are also plotted against the size of the sampled perturbations in Figures 16 and 17 for perturbations sampled from the cube and ball respectively. From these results, it is clear that additive random noise has little impact on the adversarial susceptibility of the networks, and large perturbations cause the networks’ accuracy to decrease.

It should be stressed that additive noise sampled from the cube $[-1, 1]$ (the largest cube we tested) represents a significant modification to an image where each pixel value is in $[0, 1]$. We also

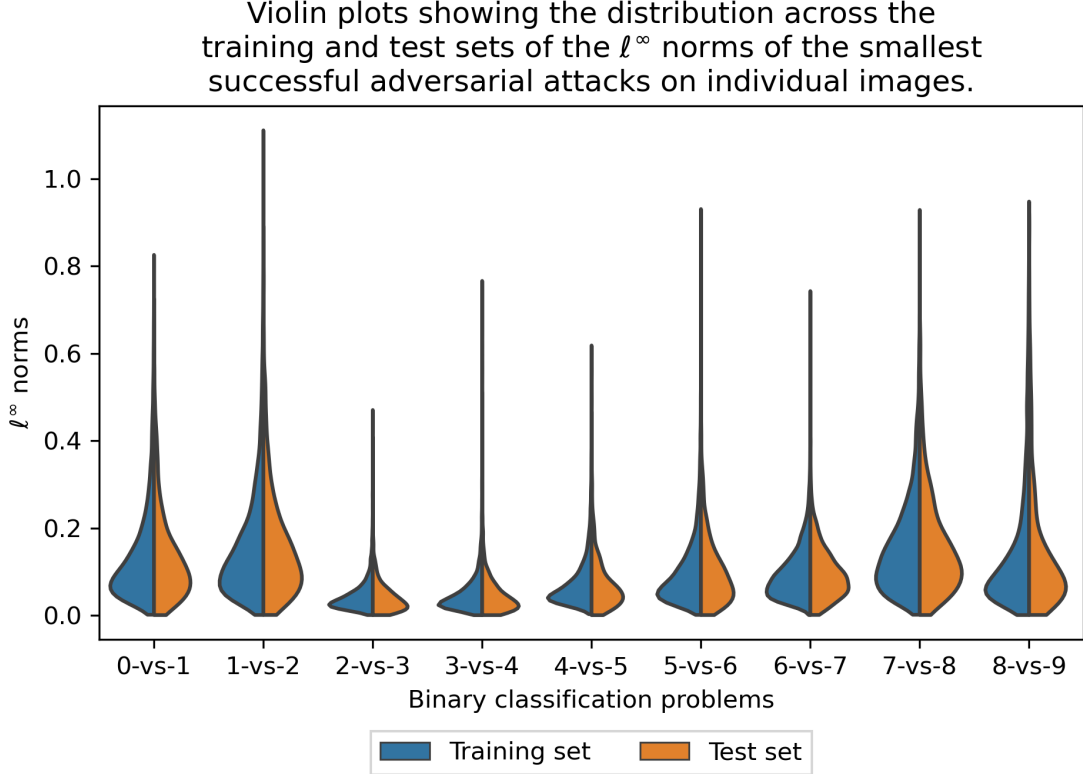


FIGURE 8. The distribution of the ℓ^∞ norms of the successful adversarial attacks found for each image using the algorithm in Section A.2, shown for a representative sample of the binary classification problems. The plotted distributions were fitted to the data using a standard Kernel Density Estimation algorithm and therefore only provide an approximation of the true empirical distribution.

	1	2	3	4	5	6	7	8	9
0	0, 0.06	0, 0.06	0, 0.06	0, 0.11	0, 0.12	0.01, 0	0.01, 0.12	0.10, 0.12	0.01, 0
1		0, 0.06	0, 0	0.01, 0.11	0, 0	0.04, 0.06	0, 0	0, 0.06	0.01, 0
2			0, 0.26	0.01, 0.06	0, 0.12	0, 0	0, 0	0, 0.06	0, 0
3				0.04, 0.12	0, 0.18	0, 0	0, 0.06	0, 0	0, 0
4					0, 0.06	0, 0.05	0, 0	0, 0.06	0.02, 0.06
5						0, 0.06	0, 0.06	0, 0	0, 0
6							0, 0	0, 0	0.01, 0.06
7								0, 0	0, 0
8									0.05, 0

TABLE 8. Susceptibility of the networks to random perturbations, as described in Section A.3 for $\delta = 1$. This is reported in the form ‘train susceptibility, test susceptibility’, where susceptibility is calculated as in (4) as the percentage of adversarially attackable images from each set which were misclassified after applying any of the 2,000 random perturbations. The row and column headers indicate the classes used in each binary classification problem. Here, we use 0 without any trailing decimal places to indicate a value which was actually zero, and not simply rounded to zero when rounding to two decimal places.

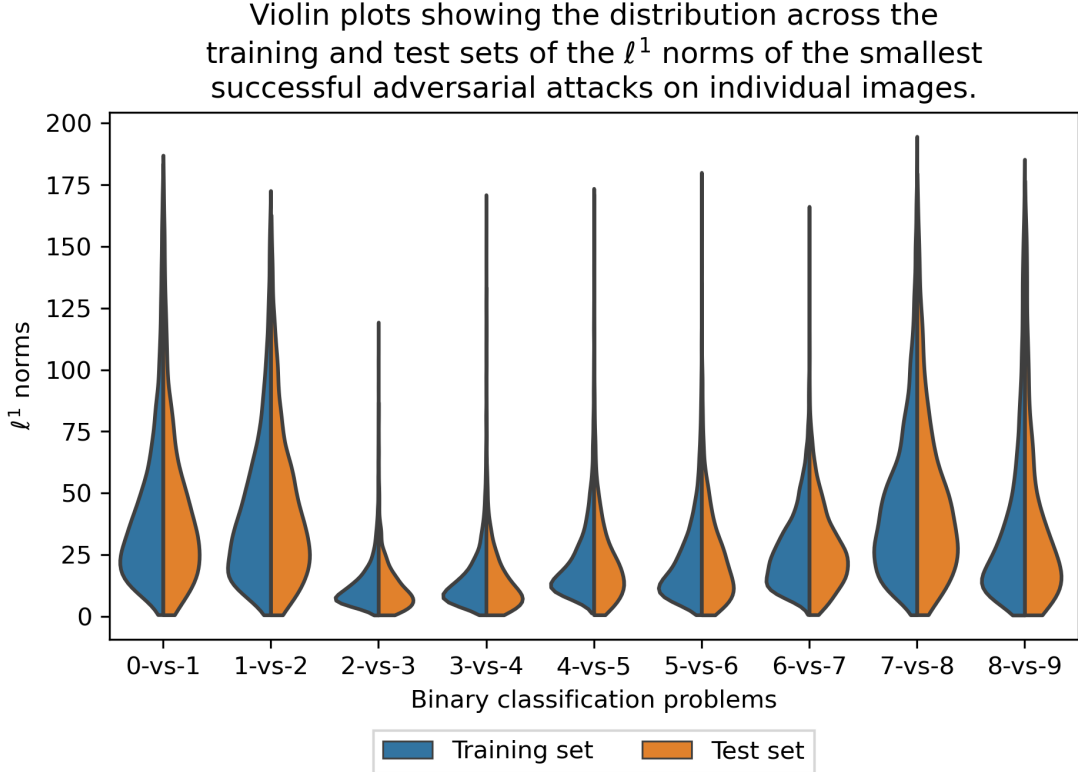


FIGURE 9. The distribution of the ℓ^1 norms of the successful adversarial attacks found for each image using the algorithm in Section A.2, shown for a representative sample of the binary classification problems. The plotted distributions were fitted to the data using a standard Kernel Density Estimation algorithm and therefore only provide an approximation of the true empirical distribution.

	1	2	3	4	5	6	7	8	9
0	0.17, 0.42	0.02, 0.06	0, 0.06	0.07, 0.17	0.04, 0.31	0.01, 0	0.04, 0.29	1.11, 1.33	0.89, 0.78
1		0.02, 0.06	0.01, 0	0.03, 0.27	0, 0	0.05, 0.06	0, 0	0.59, 0.81	0.06, 0.36
2			0.02, 0.26	0.02, 0.12	0.06, 0.24	0.07, 0.06	0.01, 0.12	0, 0.19	0, 0
3				0.11, 0.31	0.01, 0.24	0.01, 0	0, 0.06	0.01, 0	0, 0
4					0, 0.17	0.03, 0.05	0, 0.06	0.05, 0.06	0.03, 0.11
5						0.03, 0.06	0, 0.11	0.01, 0	0.03, 0.07
6							0, 0	0.03, 0	0.01, 0.06
7								0, 0	0.04, 0
8									0.97, 1.47

TABLE 9. Susceptibility of the networks to random perturbations, as described in Section A.3 for $\delta = 2$. This is reported in the form ‘train susceptibility, test susceptibility’, where susceptibility is calculated as in (4) as the percentage of adversarially attackable images from each set which were misclassified after applying any of the 2,000 random perturbations. The row and column headers indicate the classes used in each binary classification problem. Here, we use 0 without any trailing decimal places to indicate a value which was actually zero, and not simply rounded to zero when rounding to two decimal places.

	1	2	3	4	5	6	7	8	9
0	9.67, 10.56	1.55, 2.38	3.87, 4.58	9.94, 10.30	4.06, 4.93	1.75, 1.85	7.52, 8.42	8.93, 9.43	14.85, 16.57
1		7.61, 7.33	0.58, 0.25	5.99, 6.20	1.04, 1.27	1.11, 1.14	3.67, 3.12	11.06, 11.57	0.53, 0.75
2			0.12, 0.85	0.27, 0.40	0.61, 1.31	2.02, 2.46	1.65, 1.56	0.32, 0.56	2.30, 2.14
3				0.53, 0.99	0.25, 1.03	0.63, 0.63	0.23, 0.33	2.42, 2.94	0.34, 0.40
4					0.11, 0.56	0.44, 0.59	0.18, 0.56	3.46, 3.39	3.83, 3.96
5						2.97, 4.91	0.11, 0.33	2.36, 2.66	9.51, 9.74
6							0, 0.10	2.86, 3.24	0.07, 0.23
7								2.65, 2.57	1.40, 1.48
8									10.37, 10.37

TABLE 10. Susceptibility of the networks to random perturbations, as described in Section A.3 for $\delta = 5$. This is reported in the form ‘train susceptibility, test susceptibility’, where susceptibility is calculated as in (4) as the percentage of adversarially attackable images from each set which were misclassified after applying any of the 2,000 random perturbations. The row and column headers indicate the classes used in each binary classification problem. Here, we use 0 without any trailing decimal places to indicate a value which was actually zero, and not simply rounded to zero when rounding to two decimal places.

	1	2	3	4	5	6	7	8	9
0	41.49, 40.57	14.02, 16.71	29.34, 32.15	47.37, 49.55	27.49, 30.07	27.92, 28.11	50.40, 52.41	41.44, 42.16	50.82, 49.72
1		41.82, 42.67	29.38, 28.98	27.18, 28.96	41.01, 43.16	15.90, 17.79	30.90, 29.43	36.98, 36.92	29.42, 31.09
2			4.76, 6.78	16.74, 18.75	9.12, 10.48	34.10, 34.42	22.70, 23.11	19.20, 20.08	32.67, 31.80
3				5.54, 6.58	9.57, 11.04	19.86, 19.24	6.99, 8.49	28.58, 29.07	26.54, 28.01
4					5.59, 6.40	14.37, 14.77	3.87, 4.73	38.19, 39.58	31.07, 33.56
5						43.20, 42.81	6.99, 9.00	22.66, 23.23	56.10, 58.79
6							16.45, 16.70	26.87, 30.53	8.64, 8.92
7								42.90, 44.36	26.44, 26.14
8									45.04, 45.08

TABLE 11. Susceptibility of the networks to random perturbations, as described in Section A.3 for $\delta = 10$. This is reported in the form ‘train susceptibility, test susceptibility’, where susceptibility is calculated as in (4) as the percentage of adversarially attackable images from each set which were misclassified after applying any of the 2,000 random perturbations. The row and column headers indicate the classes used in each binary classification problem.

recall that the adversarial susceptibility is only calculated as the fraction of correctly classified images which are susceptible to adversarial attacks, meaning that the drop in accuracy of the classifier is implicitly decreasing the pool of images which were tested for adversarial attacks. Interestingly, the average norm of the successful adversarial attacks does seem to increase with the size of the random perturbations applied during training. However, this could once again be due to the observed drop in accuracy: training and test points which were near the decision boundary of the original classifier trained without perturbations would be those which were susceptible to the smallest adversarial attacks. These would also be the points which would be most likely to be misclassified by the less accurate classifiers trained with randomly perturbed data, so would not be included when the adversarial attacks were computed. Consequently, while large additive random noise may eliminate some of the smallest adversarial attacks, it does so at the expense of a significant drop in accuracy.

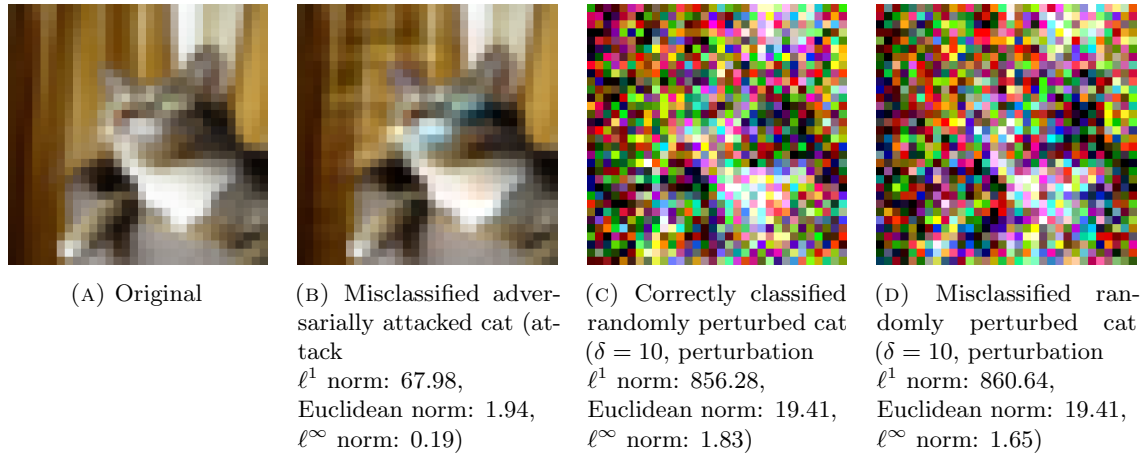


FIGURE 10. An example of an adversarially attacked image of a cat, taken from the ‘cat-vs-aeroplane’ binary classification problem (0-vs-3), alongside examples of large random perturbations to the same image which did and did not cause the network to misclassify the image. Of the 2,000 sampled random perturbations, 83 (0.0415%) caused this image to be misclassified. Components of the modified image which were outside the range $[0, 1]$ have been clipped into the range for plotting, although not for the classification.

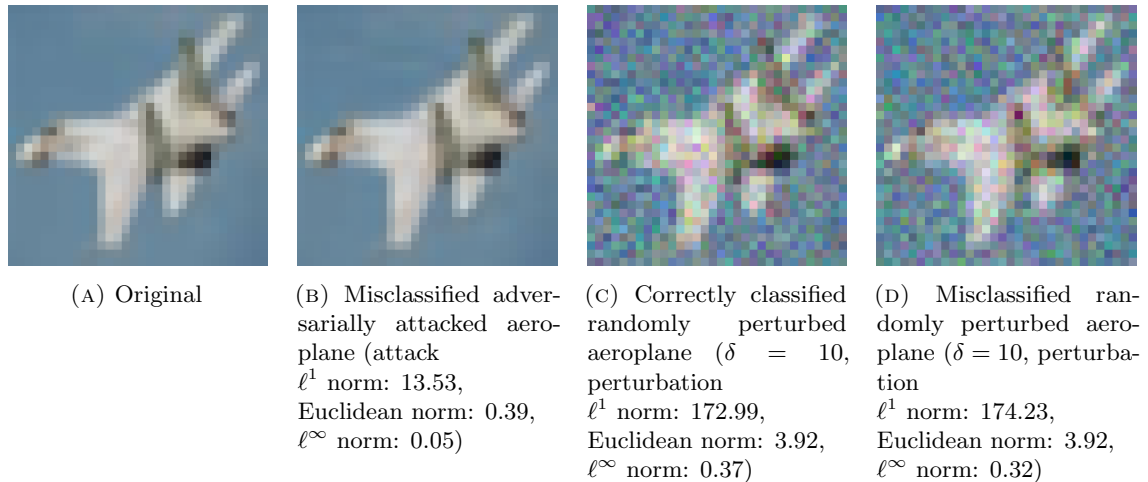


FIGURE 11. An example of an adversarially attacked image of an aeroplane, taken from the ‘cat-vs-aeroplane’ binary classification problem (0-vs-3), alongside examples of large random perturbations to the same image which did and did not cause the network to misclassify the image. Of the 2,000 sampled random perturbations, 4 (0.002%) caused this image to be misclassified. Components of the modified image which were outside the range $[0, 1]$ have been clipped into the range for plotting, although not for the classification.

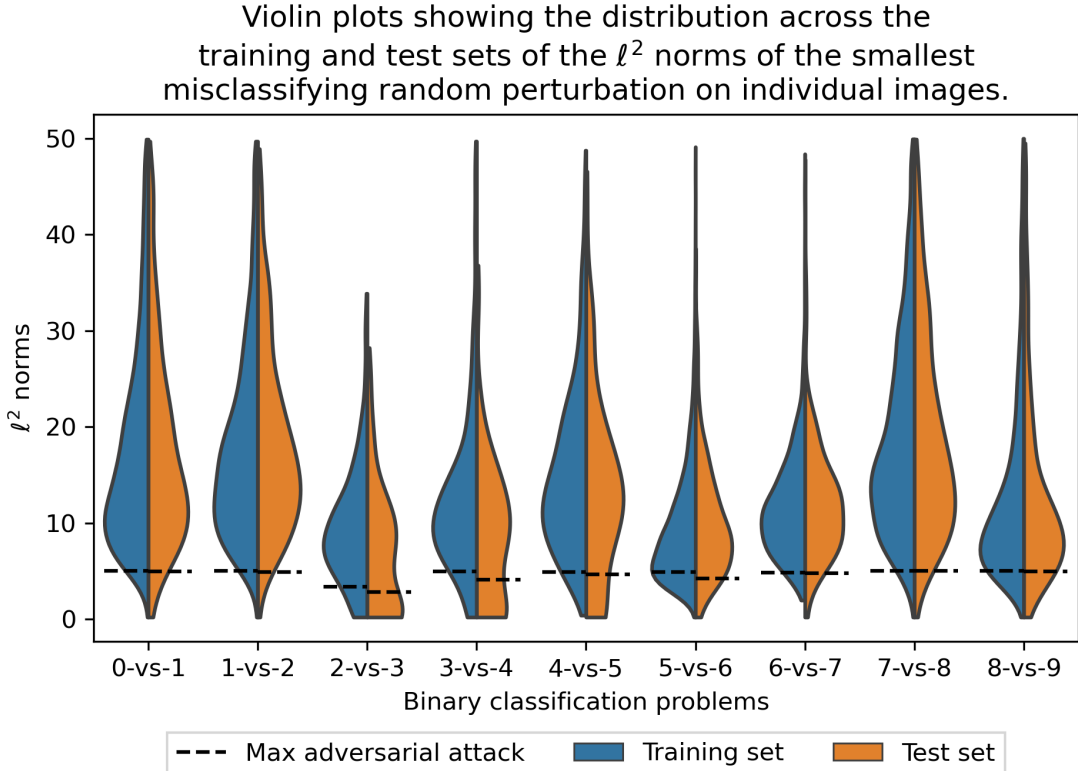


FIGURE 12. The distribution over all images in $\mathcal{X}_{i,j}^{\text{rand},10}$ (from the training set, defined in Section A.3) and $\mathcal{Y}_{i,j}^{\text{rand},10}$ (from the test set, defined in Section A.3) of the smallest Euclidean norm of a random perturbation which caused the network to misclassify the image. Black dashed lines indicate the size of the largest adversarial attack required on each data set (see Figure 7 for a plot of the full distribution of adversarial attacks). The plotted distributions were fitted to the data using a standard Kernel Density Estimation algorithm and therefore only provides an approximation of the true empirical distribution. Table 11 shows that the distributions for problems ‘2-vs-3’, ‘3-vs-4’ and ‘4-vs-5’ were constructed with fewer data points than the remaining distributions as these networks were less susceptible to random perturbations.

		0 vs 1	1 vs 2	2 vs 3	3 vs 4	4 vs 5	5 vs 6	6 vs 7	7 vs 8	8 vs 9
Accuracy	train	99.85	99.39	96.93	98.85	98.71	98.29	99.87	99.57	99.33
	test	96.40	96.60	82.45	85.90	87.45	92.45	96.35	98.05	94.75
Adv. susceptibility	train	87.85	95.14	90.49	99.96	99.46	98.67	98.87	84.85	95.94
	test	85.63	95.19	90.12	99.88	99.43	98.86	98.75	85.06	95.30
Adv. attack ℓ^1 norm	train	23.14 (35.17)	19.11 (27.94)	10.78 (17.35)	11.94 (16.84)	13.57 (18.69)	19.38 (26.04)	14.23 (19.03)	20.55 (33.22)	22.12 (32.41)
	test	23.33 (36.73)	19.75 (29.04)	10.42 (17.82)	11.92 (18.32)	12.66 (18.25)	20.58 (27.78)	14.39 (19.51)	20.68 (33.56)	22.46 (33.46)
Adv. attack ℓ^2 norm	train	0.68 (1.04)	0.57 (0.83)	0.32 (0.52)	0.34 (0.47)	0.40 (0.56)	0.59 (0.79)	0.42 (0.55)	0.60 (0.96)	0.64 (0.94)
	test	0.69 (1.08)	0.59 (0.87)	0.31 (0.54)	0.34 (0.51)	0.38 (0.54)	0.63 (0.84)	0.42 (0.57)	0.60 (0.97)	0.65 (0.97)
Adv. attack ℓ^∞ norm	train	0.07 (0.12)	0.06 (0.09)	0.03 (0.06)	0.04 (0.05)	0.04 (0.06)	0.08 (0.11)	0.05 (0.06)	0.07 (0.11)	0.08 (0.11)
	test	0.08 (0.12)	0.06 (0.10)	0.03 (0.06)	0.04 (0.06)	0.04 (0.06)	0.08 (0.11)	0.05 (0.06)	0.07 (0.11)	0.08 (0.12)

TABLE 12. Performance results when images are randomly perturbed during training using additive random noise sampled from the cube $[-a, a]^n$ with $a = 0.1$. The abbreviation ‘Adv.’ should be read as ‘Adversarial’. The quantities computed are defined in Section A. The norms of the adversarial attacks are reported in the form ‘mean (standard deviation)’, calculated by averaging over all of the correctly classified and adversarially susceptible images in each of the training and test sets.

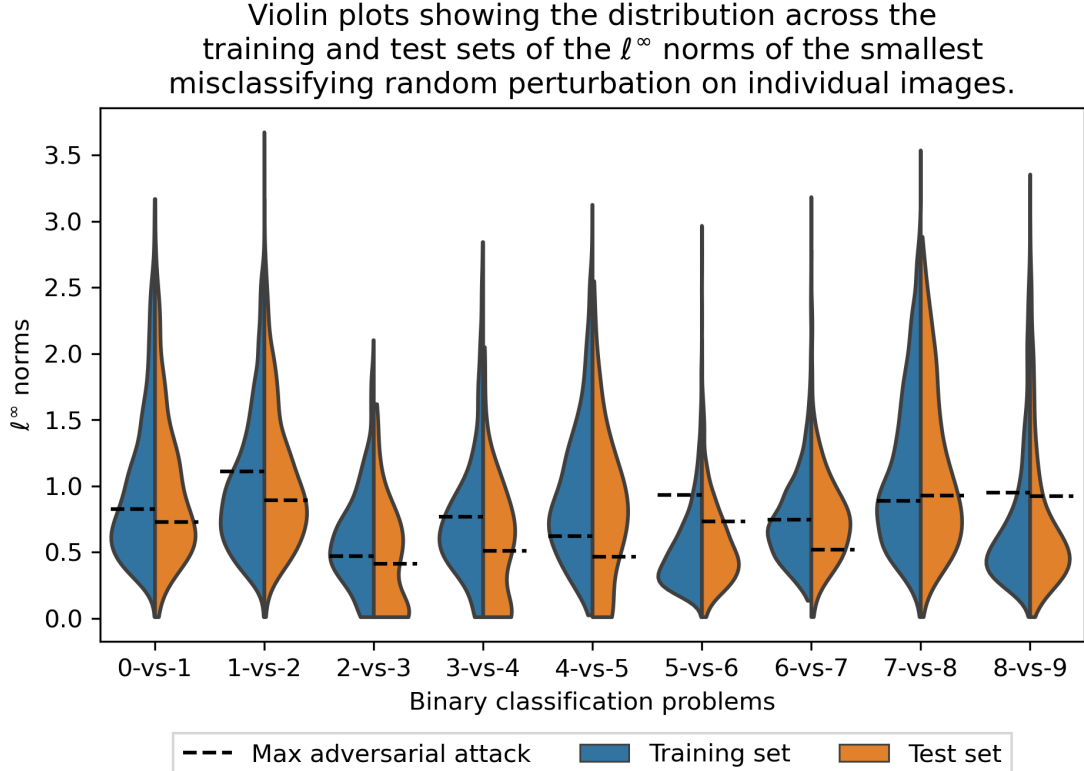


FIGURE 13. The distribution over all images in $\mathcal{X}_{i,j}^{\text{rand},10}$ (from the training set, defined in Section A.3) and $\mathcal{Y}_{i,j}^{\text{rand},10}$ (from the test set, defined in Section A.3) of the smallest ℓ^∞ norm of a random perturbation which caused the network to misclassify the image. Black dashed lines indicate the size of the largest adversarial attack required on each data set (see Figure 8 for a plot of the full distribution of adversarial attacks). The plotted distributions were fitted to the data using a standard Kernel Density Estimation algorithm and therefore only provide an approximation of the true empirical distribution. Table 11 shows that the distributions for problems ‘2-vs-3’, ‘3-vs-4’ and ‘4-vs-5’ were constructed with fewer data points than the remaining distributions as these networks were less susceptible to random perturbations.

		0 vs 1	1 vs 2	2 vs 3	3 vs 4	4 vs 5	5 vs 6	6 vs 7	7 vs 8	8 vs 9
Accuracy	train	99.83	99.69	95.33	99.02	99.39	99.45	99.82	98.64	99.45
	test	96.10	96.90	84.20	86.25	89.05	92.80	96.80	97.15	95.05
Adv. susceptibility	train	90.03	91.64	92.53	99.95	99.59	99.03	98.04	94.83	96.92
	test	88.29	91.12	92.58	100.00	99.38	98.81	97.99	94.96	96.79
Adv. attack ℓ^1 norm	train	25.16 (36.97)	18.58 (27.80)	9.94 (17.17)	11.45 (16.26)	11.95 (16.51)	17.81 (24.96)	14.97 (20.01)	22.23 (33.69)	22.58 (32.08)
	test	25.23 (37.82)	18.71 (28.24)	9.69 (16.88)	11.55 (18.15)	11.25 (16.89)	18.76 (25.94)	15.12 (21.37)	22.50 (34.12)	23.19 (33.62)
Adv. attack ℓ^2 norm	train	0.74 (1.10)	0.56 (0.83)	0.30 (0.53)	0.32 (0.46)	0.35 (0.49)	0.56 (0.78)	0.44 (0.59)	0.65 (0.99)	0.65 (0.93)
	test	0.74 (1.12)	0.56 (0.84)	0.30 (0.52)	0.33 (0.51)	0.33 (0.50)	0.58 (0.80)	0.44 (0.62)	0.66 (1.00)	0.67 (0.98)
Adv. attack ℓ^∞ norm	train	0.08 (0.13)	0.06 (0.10)	0.04 (0.07)	0.03 (0.05)	0.04 (0.06)	0.07 (0.11)	0.05 (0.07)	0.07 (0.12)	0.08 (0.11)
	test	0.08 (0.13)	0.06 (0.10)	0.04 (0.07)	0.03 (0.06)	0.04 (0.06)	0.08 (0.11)	0.05 (0.07)	0.07 (0.12)	0.08 (0.12)

TABLE 13. Performance results when images are randomly perturbed during training using additive random noise sampled from the ball \mathbb{B}_b^n with $b = 3.2$. The abbreviation ‘Adv.’ should be read as ‘Adversarial’. The quantities computed are defined in Section A. The norms of the adversarial attacks are reported in the form ‘mean (standard deviation)’, calculated by averaging over all of the correctly classified and adversarially susceptible images in each of the training and test sets.

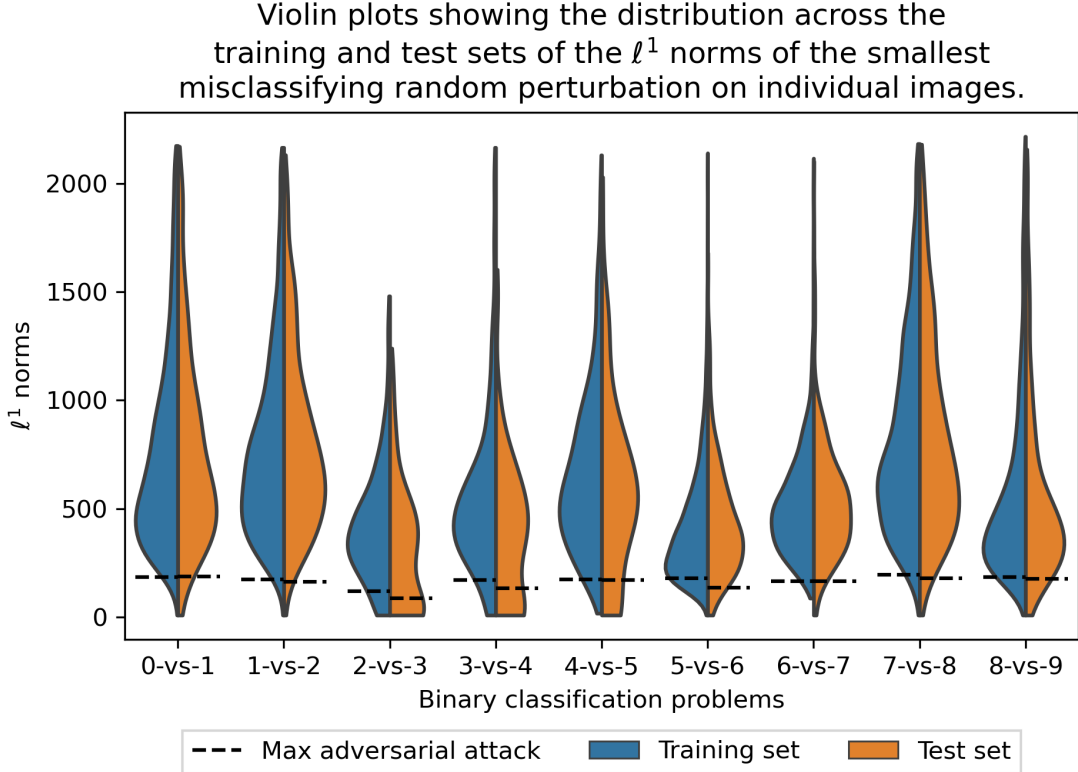


FIGURE 14. The distribution over all images in $\mathcal{X}_{i,j}^{\text{rand},10}$ (from the training set, defined in Section A.3) and $\mathcal{Y}_{i,j}^{\text{rand},10}$ (from the test set, defined in Section A.3) of the smallest ℓ^1 norm of a random perturbation which caused the network to misclassify the image. Black dashed lines indicate the size of the largest adversarial attack required on each data set (see Figure 9 for a plot of the full distribution of adversarial attacks). The plotted distributions were fitted to the data using a standard Kernel Density Estimation algorithm and therefore only provide an approximation of the true empirical distribution. Table 11 shows that the distributions for problems ‘2-vs-3’, ‘3-vs-4’ and ‘4-vs-5’ were constructed with fewer data points than the remaining distributions as these networks were less susceptible to random perturbations.

		0 vs 1	1 vs 2	2 vs 3	3 vs 4	4 vs 5	5 vs 6	6 vs 7	7 vs 8	8 vs 9
Accuracy	train	92.82	94.43	91.57	92.89	95.75	94.60	98.96	97.50	89.54
	test	89.50	92.05	81.50	82.80	86.95	88.80	94.65	95.40	85.35
Adv. susceptibility	train	76.02	98.56	98.21	99.26	98.55	94.27	99.20	95.57	83.88
	test	74.36	98.32	97.98	99.03	98.45	93.24	99.26	95.07	83.54
Adv. attack ℓ^1 norm	train	35.56 (50.17)	21.88 (33.12)	24.70 (34.77)	22.03 (33.51)	28.38 (35.91)	28.85 (37.80)	22.88 (29.34)	27.83 (39.89)	45.61 (55.12)
	test	35.17 (50.80)	21.82 (32.95)	25.02 (36.26)	21.81 (33.94)	27.13 (35.90)	29.06 (38.87)	23.70 (31.22)	27.50 (39.63)	45.39 (54.85)
Adv. attack ℓ^2 norm	train	1.01 (1.44)	0.65 (0.98)	0.70 (1.00)	0.61 (0.91)	0.82 (1.04)	0.87 (1.13)	0.67 (0.85)	0.78 (1.11)	1.27 (1.53)
	test	1.01 (1.47)	0.65 (0.98)	0.71 (1.04)	0.60 (0.93)	0.78 (1.04)	0.88 (1.17)	0.69 (0.91)	0.77 (1.10)	1.27 (1.53)
Adv. attack ℓ^∞ norm	train	0.10 (0.15)	0.07 (0.11)	0.07 (0.10)	0.06 (0.09)	0.08 (0.11)	0.10 (0.13)	0.07 (0.09)	0.08 (0.12)	0.13 (0.17)
	test	0.11 (0.16)	0.07 (0.11)	0.07 (0.11)	0.06 (0.09)	0.08 (0.11)	0.10 (0.13)	0.07 (0.10)	0.08 (0.12)	0.13 (0.17)

TABLE 14. Performance results when images are randomly perturbed during training using additive random noise sampled from the cube $[-a, a]^n$ with $a = 0.5$. The abbreviation ‘Adv.’ should be read as ‘Adversarial’. The quantities computed are defined in Section A. The norms of the adversarial attacks are reported in the form ‘mean (standard deviation)’, calculated by averaging over all of the correctly classified and adversarially susceptible images in each of the training and test sets.

Violin plots showing the distribution across the training and test sets of the norms of (1) smallest successful adversarial attacks, and (2) smallest misclassifying random perturbation on individual images.

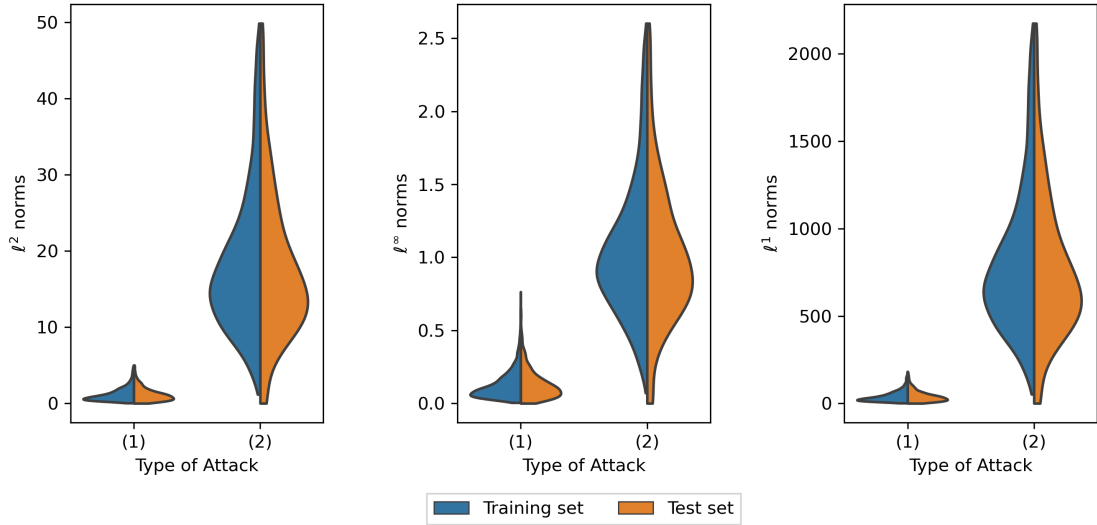


FIGURE 15. A direct comparison of the size distributions over all attackable images in the training and test sets of the smallest successful adversarial attack and smallest misclassifying random perturbation for the ‘cat-vs-aeroplane’ problem (0-vs-3), as measured in various norms. The plotted distributions were fitted to the data using a standard Kernel Density Estimation algorithm and therefore only provide an approximation of the true empirical distribution.

		0 vs 1	1 vs 2	2 vs 3	3 vs 4	4 vs 5	5 vs 6	6 vs 7	7 vs 8	8 vs 9
Accuracy	train	95.08	96.21	88.05	93.85	96.42	90.75	98.97	97.06	89.75
	test	91.10	94.40	78.30	82.30	85.45	85.65	94.95	95.50	85.45
Adv. susceptibility	train	79.44	97.78	93.16	99.38	99.16	92.32	99.36	96.46	85.86
	test	77.22	97.72	92.40	99.45	99.06	90.37	99.53	96.07	85.08
Adv. attack ℓ^1 norm	train	34.08 (47.83)	25.09 (36.56)	32.75 (41.78)	20.49 (31.84)	26.35 (34.00)	33.95 (41.52)	24.59 (31.05)	30.17 (42.56)	47.84 (56.68)
	test	32.84 (46.83)	24.62 (36.20)	32.60 (42.07)	20.69 (33.00)	25.62 (34.86)	33.66 (42.43)	25.21 (32.42)	29.99 (42.89)	46.48 (55.40)
Adv. attack ℓ^2 norm	train	0.99 (1.40)	0.74 (1.07)	0.93 (1.19)	0.56 (0.87)	0.76 (0.98)	1.02 (1.24)	0.71 (0.89)	0.83 (1.17)	1.33 (1.57)
	test	0.97 (1.39)	0.73 (1.06)	0.93 (1.20)	0.57 (0.90)	0.74 (1.00)	1.01 (1.26)	0.73 (0.93)	0.83 (1.17)	1.29 (1.54)
Adv. attack ℓ^∞ norm	train	0.10 (0.15)	0.08 (0.11)	0.10 (0.13)	0.06 (0.09)	0.08 (0.10)	0.12 (0.14)	0.07 (0.09)	0.09 (0.12)	0.14 (0.17)
	test	0.10 (0.15)	0.07 (0.11)	0.09 (0.13)	0.06 (0.09)	0.07 (0.10)	0.11 (0.14)	0.07 (0.10)	0.08 (0.12)	0.13 (0.16)

TABLE 15. Performance results when images are randomly perturbed during training using additive random noise sampled from the ball \mathbb{B}_b^n with $b = 16$. The abbreviation ‘Adv.’ should be read as ‘Adversarial’. The quantities computed are defined in Section A. The norms of the adversarial attacks are reported in the form ‘mean (standard deviation)’, calculated by averaging over all of the correctly classified and adversarially susceptible images in each of the training and test sets.

APPENDIX C. PROOFS OF MAIN THEOREMS

C.1. Proof of Theorem 2. Expanding the probability using the definition of the distribution \mathcal{D}_ϵ , and the definition of the classifier f , we have

$$\begin{aligned} P((x, \ell) \sim \mathcal{D}_\epsilon : f(x) = \ell) \\ = \frac{1}{2} P(x \sim \mathcal{D}_0 : f(x) = 0) + \frac{1}{2} P(x \sim \mathcal{D}_1 : f(x) = 1) \end{aligned}$$

The factor of $\frac{1}{2}$ is due to the fact that samples with either label are sampled with equal probability. Negating these two probabilities and expressing them as integrals using the densities p_0 and p_1 associated with \mathcal{D}_0 and \mathcal{D}_1 respectively (the existence of these densities is a requirement of the

		0 vs 1	1 vs 2	2 vs 3	3 vs 4	4 vs 5	5 vs 6	6 vs 7	7 vs 8	8 vs 9
Accuracy	train	85.65	89.84	82.44	85.20	85.20	90.75	93.56	94.50	76.09
	test	84.00	88.40	76.40	80.40	81.30	87.75	91.15	92.45	74.60
Adv. susceptibility	train	75.66	98.90	93.92	97.79	93.96	97.41	98.57	96.96	61.51
	test	74.40	98.81	92.41	98.07	93.97	97.26	98.08	97.13	61.93
Adv. attack ℓ^1 norm	train	47.29 (60.24)	22.74 (35.90)	38.53 (49.56)	25.62 (41.16)	46.07 (52.80)	26.32 (39.04)	39.02 (45.31)	31.71 (44.80)	55.25 (68.60)
	test	45.52 (58.87)	22.06 (35.82)	38.01 (49.77)	25.61 (41.41)	45.18 (52.78)	27.85 (41.27)	39.61 (46.00)	31.00 (44.60)	54.28 (67.73)
Adv. attack ℓ^2 norm	train	1.29 (1.64)	0.66 (1.04)	1.06 (1.36)	0.67 (1.08)	1.29 (1.48)	0.77 (1.14)	1.12 (1.30)	0.86 (1.21)	1.44 (1.78)
	test	1.25 (1.61)	0.64 (1.03)	1.05 (1.36)	0.67 (1.08)	1.26 (1.47)	0.82 (1.21)	1.13 (1.31)	0.84 (1.21)	1.41 (1.76)
Adv. attack ℓ^∞ norm	train	0.12 (0.15)	0.07 (0.11)	0.10 (0.13)	0.06 (0.10)	0.13 (0.15)	0.08 (0.12)	0.11 (0.13)	0.08 (0.12)	0.13 (0.16)
	test	0.11 (0.15)	0.06 (0.10)	0.10 (0.13)	0.06 (0.10)	0.12 (0.15)	0.08 (0.13)	0.11 (0.13)	0.08 (0.12)	0.12 (0.16)

TABLE 16. Performance results when images are randomly perturbed during training using additive random noise sampled from the cube $[-a, a]^n$ with $a = 1$. The abbreviation ‘Adv.’ should be read as ‘Adversarial’. The quantities computed are defined in Section A. The norms of the adversarial attacks are reported in the form ‘mean (standard deviation)’, calculated by averaging over all of the correctly classified and adversarially susceptible images in each of the training and test sets.

		0 vs 1	1 vs 2	2 vs 3	3 vs 4	4 vs 5	5 vs 6	6 vs 7	7 vs 8	8 vs 9
Accuracy	train	86.82	91.61	84.19	85.79	84.17	90.45	94.29	93.40	80.22
	test	84.55	89.85	78.55	80.25	80.80	88.10	91.35	91.20	77.25
Adv. susceptibility	train	72.14	98.50	94.35	98.18	92.23	97.63	98.26	98.73	68.44
	test	71.08	98.16	93.19	98.32	92.51	97.73	98.14	98.85	68.41
Adv. attack ℓ^1 norm	train	43.25 (58.85)	25.08 (38.16)	34.84 (47.12)	25.38 (40.59)	48.40 (54.21)	25.85 (39.18)	38.47 (45.03)	29.10 (42.32)	53.87 (66.98)
	test	42.76 (58.44)	24.30 (37.83)	34.82 (48.19)	25.47 (40.99)	46.92 (53.64)	27.88 (42.30)	39.74 (46.60)	28.83 (42.06)	54.82 (67.20)
Adv. attack ℓ^2 norm	train	1.18 (1.61)	0.72 (1.09)	0.95 (1.28)	0.67 (1.06)	1.36 (1.52)	0.75 (1.12)	1.10 (1.29)	0.78 (1.13)	1.41 (1.75)
	test	1.18 (1.61)	0.69 (1.07)	0.95 (1.31)	0.67 (1.07)	1.32 (1.50)	0.81 (1.22)	1.13 (1.33)	0.77 (1.13)	1.43 (1.76)
Adv. attack ℓ^∞ norm	train	0.11 (0.15)	0.07 (0.11)	0.09 (0.12)	0.06 (0.09)	0.13 (0.16)	0.07 (0.11)	0.10 (0.13)	0.07 (0.11)	0.13 (0.16)
	test	0.11 (0.16)	0.07 (0.11)	0.09 (0.13)	0.06 (0.09)	0.13 (0.15)	0.08 (0.12)	0.11 (0.13)	0.07 (0.11)	0.13 (0.16)

TABLE 17. Performance results when images are randomly perturbed during training using additive random noise sampled from the ball \mathbb{B}_b^n with $b = 32$. The abbreviation ‘Adv.’ should be read as ‘Adversarial’. The quantities computed are defined in Section A. The norms of the adversarial attacks are reported in the form ‘mean (standard deviation)’, calculated by averaging over all of the correctly classified and adversarially susceptible images in each of the training and test sets.

SmAC property), we have

$$\begin{aligned} P((x, \ell) \sim \mathcal{D}_\epsilon : f(x) = \ell) \\ = 1 - \frac{1}{2} \int_{D_0} \mathbb{I}_{\{x_1 > 0\}} p_0(x) dx - \frac{1}{2} \int_{D_1} \mathbb{I}_{\{x_1 < 0\}} p_1(x) dx. \end{aligned}$$

The bound on the density p provided by the SmAC property in Definition 1 (recalling that $r = 1$ for both distributions) therefore implies that

$$\begin{aligned} P((x, \ell) \sim \mathcal{D}_\epsilon : f(x) = \ell) \\ \geq 1 - \frac{A^n}{2V^n} \left(\int_{D_0} \mathbb{I}_{\{x_1 > 0\}} dx + \int_{D_1} \mathbb{I}_{\{x_1 < 0\}} dx \right). \end{aligned}$$

By symmetry, the two integrals have the same value, so we only compute the first. Since $\epsilon > 0$, this corresponds to the volume of a section of a ball which is smaller than a hemisphere, we may write it as

$$\int_{D_0} \mathbb{I}_{\{x_1 > 0\}} dx = V_{\text{cap}}^n(1, 1 - \epsilon).$$

Enveloping the spherical cap in a hemisphere shows the following lemma.

Lemma 9 (Spherical cap volume bound). *Let n be a positive integer, and $r \geq h > 0$. Then,*

$$V_{\text{cap}}^n(r, h) \leq \frac{1}{2} V^n r^n \left(1 - \left(1 - \frac{h}{r} \right)^2 \right)^{\frac{n}{2}}.$$

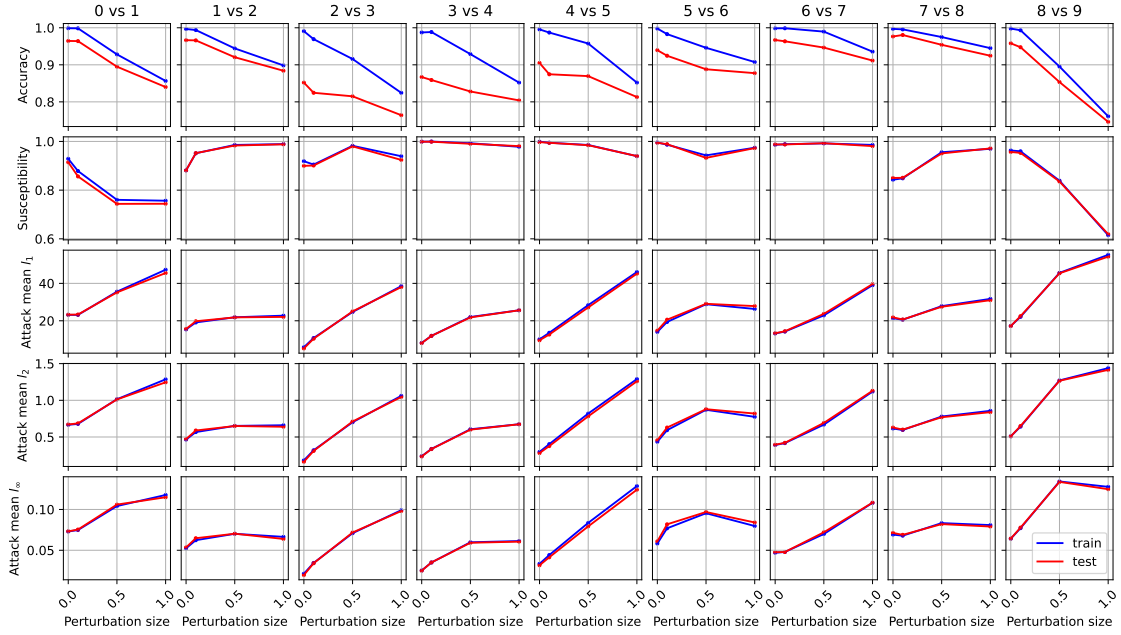


FIGURE 16. Plots showing how the performance of the network is affected by various magnitudes of random perturbations added to the images during training. This figure shows the results for random perturbations sampled from the cube $[-a, a]^n$ for $a \in \{0, 0.1, 0.5, 1\}$. This visualises the results in Tables 12, 14 and 16 compared to the previous data computed with no random perturbations (corresponding to $a = 0$). The data is plotted as separate lines for the training and test sets. ‘Susceptibility’ here refers to the adversarial susceptibility reported in the tables, and ‘Attack mean ℓ_p ’ indicates the mean across each data set of the ℓ^p norm of the smallest adversarial perturbation affecting each image. The perturbation size plotted on the x axis is the size of a .

This implies that

$$V_{\text{cap}}^n(1, 1 - \epsilon) \leq \frac{1}{2} V^n (1 - \epsilon^2)^{\frac{n}{2}},$$

and the result therefore follows.

C.2. Proof of Theorem 3. Using the definition of the classification function f and conditioning on the class label, we may rewrite the probability in question as

$$\begin{aligned} P((x, \ell) \sim \mathcal{D}_\epsilon : \text{there exists } s \in \mathbb{B}_\delta^n \text{ such that } f(x + s) \neq \ell) \\ = \frac{1}{2} P(x \sim \mathcal{U}(D_0) : x_1 > -\delta) + \frac{1}{2} P(x \sim \mathcal{U}(D_1) : x_1 < \delta). \end{aligned}$$

Symmetry implies that these two probabilities have the same value, so we only need to compute the first one. Negating the probability and expanding it as an integral using the density p_0 of D_0 , we find that

$$P(x \sim \mathcal{U}(D_0) : x_1 > -\delta) = 1 - \int_{D_0} \mathbb{I}_{\{x_1 < -\delta\}} p_0(x) dx.$$

The bound on the density provided by the SmAC property (Definition 1) therefore implies that

$$P(x \sim \mathcal{U}(D_0) : x_1 > -\delta) \geq 1 - \frac{A^n}{V^n} \int_{D_0} \mathbb{I}_{\{x_1 < -\delta\}} dx.$$

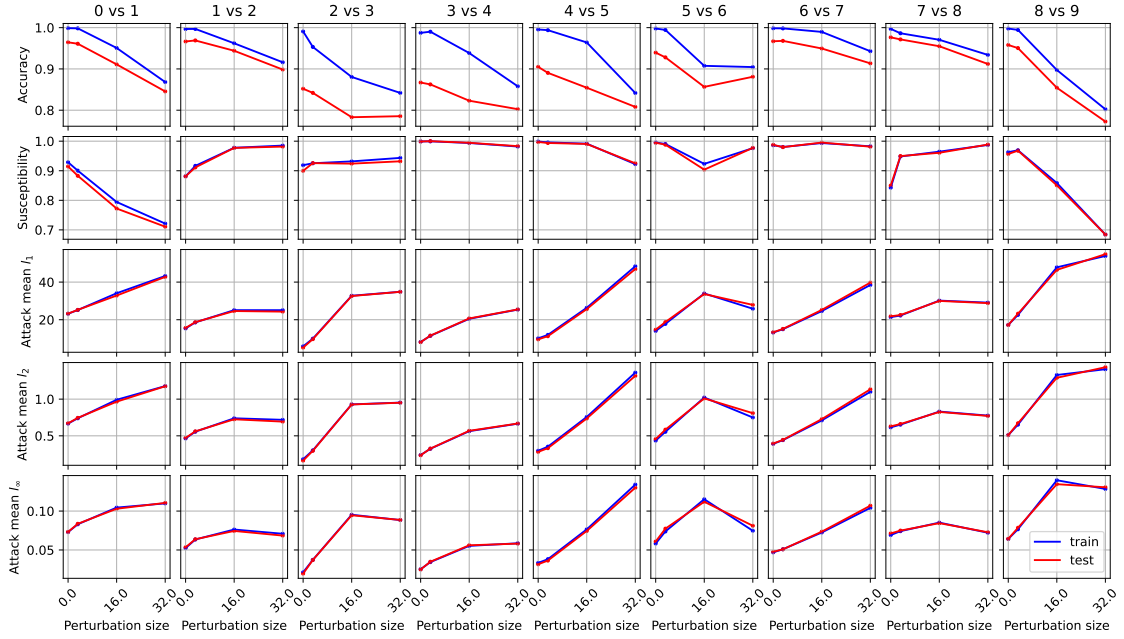


FIGURE 17. Plots showing how the performance of the network is affected by various magnitudes of random perturbations added to the images during training. This figure shows the results for random perturbations sampled from the ball \mathbb{B}_b^n for $b \in \{0, 3.2, 16, 32\}$. This visualises the results in Tables 12, 14 and 16 compared to the previous data computed with no random perturbations (corresponding to $b = 0$). The data is plotted as separate lines for the training and test sets. ‘Susceptibility’ here refers to the adversarial susceptibility reported in the tables, and ‘Attack mean ℓ_p ’ indicates the mean across each data set of the ℓ^p norm of the smallest adversarial perturbation affecting each image. The perturbation size plotted on the x axis is the size of a .

Since this integral corresponds to the volume of a spherical cap with height smaller than its radius (due to the fact that $1 > \delta > \epsilon > 0$), we may apply Lemma 9 to show that

$$\begin{aligned} \int_{D_0} \mathbb{I}_{\{x_1 < -\delta\}} dx &= V_{\text{cap}}^n(1, 1 - (\epsilon - \delta)) \\ &\leq \frac{1}{2} V^n (1 - (\delta - \epsilon)^2)^{\frac{n}{2}}, \end{aligned}$$

and the result therefore follows.

C.3. Proof of Theorem 4. To prove Theorem 4, we begin by expanding the probability by conditioning on the label value, finding

$$\begin{aligned} &P((x, \ell) \sim \mathcal{D}_\epsilon, s \sim \mathcal{U}(\mathbb{B}_\delta^n) : f(x + s) \neq \ell) \\ &= \frac{1}{2} P(x \sim \mathcal{U}(D_0), s \sim \mathcal{U}(\mathbb{B}_\delta^n) : x_1 + s_1 > 0) \\ &\quad + \frac{1}{2} P(x \sim \mathcal{U}(D_1), s \sim \mathcal{U}(\mathbb{B}_\delta^n) : x_1 + s_1 < 0). \end{aligned}$$

The symmetry here implies that these two probabilities are equal, so we proceed by only bounding the first. Expanding this as an integral using the density p_0 of D_0 and the fact that s is sampled

from a uniform distribution, we observe that

$$\begin{aligned} P(x \sim \mathcal{U}(D_0), s \sim \mathcal{U}(\mathbb{B}_\delta^n) : x_1 + s_1 > 0) \\ = \frac{1}{V^n \delta^n} \int_{D_0} \int_{\mathbb{B}_\delta^n} \mathbb{I}_{\{s_1 > -x_1\}} ds p_0(x) dx. \end{aligned}$$

The bound on the density provided by the SmAC property (Definition 1) therefore implies that

$$\begin{aligned} P(x \sim \mathcal{U}(D_0), s \sim \mathcal{U}(\mathbb{B}_\delta^n) : x_1 + s_1 > 0) \\ \leq \frac{A^n}{(V^n)^2 \delta^n} \int_{D_0} \int_{\mathbb{B}_\delta^n} \mathbb{I}_{\{s_1 > -x_1\}} ds dx. \end{aligned}$$

For each fixed value of x , the inner integral is just computing the volume of a section of a ball with radius δ . When $x_1 > 0$, this volume is at least a hemisphere, while when $x_1 < 0$ this volume is less than a hemisphere. On the other hand, for fixed s , the integral over x is also calculating the volume of a section of the unit ball. Since the volume of the ball concentrates in high dimensions about its equator, a section which is smaller than a hemisphere may be expected to have small volume, while a section larger than a hemisphere may be expected to have large volume. This is the intuition we apply here by splitting the integral into two parts: one for $x_1 < -t$ and one for $x_1 \geq -t$ for some arbitrary $t \in [0, \epsilon]$. In the first part, we will be able to obtain ‘smallness’ in our bound from the fact that we are integrating s over just a spherical cap, while in the second case we are integrating x over a spherical cap. We write this splitting as

$$\begin{aligned} (5) \quad & \int_{D_0} \int_{\mathbb{B}_\delta^n} \mathbb{I}_{\{s_1 > -x_1\}} ds dx \\ & = \int_{D_0} \int_{\mathbb{B}_\delta^n} \mathbb{I}_{\{x_1 < -t\}} \mathbb{I}_{\{s_1 > -x_1\}} ds dx \\ & \quad + \int_{D_0} \int_{\mathbb{B}_\delta^n} \mathbb{I}_{\{x_1 > -t\}} \mathbb{I}_{\{s_1 > -x_1\}} ds dx. \end{aligned}$$

The first term of this splitting may be bounded above by extending the indicator function over s to all those points with $s_1 > t$ (since $-x_1 > t$), which enables us to separate the integrals to find that

$$\begin{aligned} & \int_{D_0} \int_{\mathbb{B}_\delta^n} \mathbb{I}_{\{x_1 < -t\}} \mathbb{I}_{\{s_1 > -x_1\}} ds dx \\ & \leq \int_{D_0} \mathbb{I}_{\{x_1 < -t\}} dx \int_{\mathbb{B}_\delta^n} \mathbb{I}_{\{s_1 > t\}} ds. \end{aligned}$$

These integrals may be expressed as volumes in the form

$$\begin{aligned} & \int_{D_0} \mathbb{I}_{\{x_1 < -t\}} dx \int_{\mathbb{B}_\delta^n} \mathbb{I}_{\{s_1 > t\}} ds \\ & = (V^n - V_{\text{cap}}^n(1, 1 - (\epsilon - t))) V_{\text{cap}}^n(\delta, \delta - t), \end{aligned}$$

and Lemma 9 and the fact that the volume of a spherical cap is non-negative implies that

$$\int_{D_0} \mathbb{I}_{\{x_1 < -t\}} dx \int_{\mathbb{B}_\delta^n} \mathbb{I}_{\{s_1 > t\}} ds \leq \frac{1}{2} (V^n)^2 \delta^n \left(1 - \left(\frac{t}{\delta}\right)^2\right)^{\frac{n}{2}}.$$

Returning to the second integral in (5), we may similarly bound the indicator function over s from above by simply the constant 1. This implies that

$$\begin{aligned} & \int_{D_0} \int_{\mathbb{B}_\delta^n} \mathbb{I}_{\{x_1 > -t\}} \mathbb{I}_{\{s_1 > -x_1\}} ds dx \leq \int_{D_0} \mathbb{I}_{\{x_1 > -t\}} dx \int_{\mathbb{B}_\delta^n} ds \\ & = V_{\text{cap}}^n(1, 1 - (\epsilon - t)) V^n \delta^n, \end{aligned}$$

and Lemma 9 consequently provides

$$\begin{aligned} & \int_{D_0} \int_{\mathbb{B}_\delta^n} \mathbb{I}_{\{x_1 > -t\}} \mathbb{I}_{\{s_1 > -x_1\}} ds dx \\ & \leq \frac{1}{2} (V^n)^2 \delta^n (1 - (\epsilon - t)^2)^{\frac{n}{2}}. \end{aligned}$$

Combining these bounds and using the fact that $t \in [0, \epsilon]$ was arbitrary, we find that

$$\begin{aligned} & P((x, \ell) \sim \mathcal{D}_\epsilon, s \sim \mathcal{U}(\mathbb{B}_\delta^n) : f(x + s) \neq \ell) \\ & \leq \frac{1}{2} A^n \inf_{t \in [0, \epsilon]} \left[\left(1 - \left(\frac{t}{\delta}\right)^2\right)^{\frac{n}{2}} + (1 - (\epsilon - t)^2)^{\frac{n}{2}} \right], \end{aligned}$$

and the theorem follows by noting that, for $t = \frac{\epsilon\delta}{1+\delta}$, the two terms inside the infimum are equal (this choice of t is valid since $\frac{\delta}{1+\delta} \in [0, 1]$ for $\delta \geq 0$).

C.4. Proof of Theorem 5. Since the statement and setup are symmetric with respect to the class label ℓ , we focus only on the class 0 and the statement for class 1 follows analogously. In this case, the statement that

$$f(x + s) \neq \ell \text{ for all } s \in \mathbb{R}^n \text{ such that } d_\ell(z, s) > \gamma,$$

is implied by the condition that $z_1 < x_1 + \gamma$, and therefore

$$\begin{aligned} & P(x, z \sim \mathcal{U}(D_0) : f(x + s) \neq 0 \text{ for all } s \in \mathbb{R}^n \\ & \quad \text{such that } d_0(z, s) > \gamma) \\ & \geq P(x, z \sim \mathcal{U}(D_0) : z_1 < x_1 + \gamma). \end{aligned}$$

Negating this probability and expressing this probability as an integral using the density p_0 of D_0 , we find that

$$\begin{aligned} & P(x, z \sim \mathcal{U}(D_0) : z_1 < x_1 + \gamma) \\ & = 1 - \int_{D_0} \int_{D_0} \mathbb{I}_{\{z_1 > x_1 + \gamma\}} p_0(z) dz p_0(x) dx, \end{aligned}$$

and therefore, using the bound on the density provided by Definition 1 with $r = 1$, we obtain the lower bound

$$\begin{aligned} & P(x, z \sim \mathcal{U}(D_0) : z_1 < x_1 + \gamma) \\ & \geq 1 - A^{2n} + \left(\frac{A^n}{V^n}\right)^2 \int_{D_0} \int_{D_0} \mathbb{I}_{\{z_1 < x_1 + \gamma\}} dz dx, \end{aligned}$$

Introducing $t \in [0, \gamma]$, we may split the integral over x as

$$\begin{aligned} & \int_{D_0} \int_{D_0} \mathbb{I}_{\{z_1 < x_1 + \gamma\}} dz dx \\ & = \int_{D_0} \mathbb{I}_{\{x_1 < -\epsilon - t\}} \int_{D_0} \mathbb{I}_{\{z_1 < x_1 + \gamma\}} dz dx \\ & \quad + \int_{D_0} \mathbb{I}_{\{x_1 > -\epsilon - t\}} \int_{D_0} \mathbb{I}_{\{z_1 < x_1 + \gamma\}} dz dx. \end{aligned}$$

The first term on the right hand side of this is trivially greater than or equal to zero. For the second term, we observe that the condition $x_1 > -\epsilon - t$ implies that the set of $z \in D_0$ such that $z_1 < x_1 + \gamma$ is greater than a hemisphere. We may express the integral over z in the form

$$\begin{aligned} & \int_{D_0} \mathbb{I}_{\{z_1 < x_1 + \gamma\}} dz = V^n - V_{\text{cap}}^n(1, 1 - (x_1 + \gamma + \epsilon)) \\ & \geq V^n \left(1 - \frac{1}{2} (1 - (\gamma - t)^2)^{\frac{n}{2}}\right), \end{aligned}$$

where the lower bound is due to Lemma 9 and the bound on x_1 . We therefore find that

$$\begin{aligned} & \int_{D_0} \mathbb{I}_{\{x_1 > -\epsilon - t\}} \int_{D_0} \mathbb{I}_{\{z_1 < x_1 + \gamma\}} dz dx \\ & \geq V^n \int_{D_0} \mathbb{I}_{\{x_1 > -\epsilon - t\}} dx \left(1 - \frac{1}{2}(1 - (\gamma - t)^2)^{\frac{n}{2}}\right), \end{aligned}$$

and, since the integral over x is now just the volume of a ball missing a spherical cap, arguing as above shows that

$$\begin{aligned} \int_{D_0} \mathbb{I}_{\{x_1 > -\epsilon - t\}} dx &= V^n - V_{\text{cap}}^n(1, 1 - t) \\ &\geq V^n \left(1 - \frac{1}{2}(1 - t^2)^{\frac{n}{2}}\right), \end{aligned}$$

since $t \in [0, \gamma]$. Consequently, because t was arbitrary, we conclude that

$$\begin{aligned} P(x, z \sim \mathcal{U}(D_0) : x_1 > z_1 - \gamma) \\ \geq 1 - A^{2n} \left[1 - \inf_{t \in [0, \gamma]} \left(1 - \frac{1}{2}(1 - (\gamma - t)^2)^{\frac{n}{2}}\right) \cdot \left(1 - \frac{1}{2}(1 - t^2)^{\frac{n}{2}}\right)\right], \end{aligned}$$

and the theorem follows by observing that the two terms in the infimum are balanced for $t = \frac{\gamma}{2}$.

C.5. Proof of Theorem 6. When $\ell = 0$, we have $|\tilde{f}(x) - \ell| = \sigma(g(x))$, since $\sigma(t) \in (0, 1)$ for $t \in \mathbb{R}$. In this case, the attack may therefore be computed as

$$\mathbf{e}_1 \sigma'(g(x)) L'(\sigma(g(x))),$$

since $g'(x) = \mathbf{e}_1$. Since $\sigma'(t), L'(t) > 0$ by assumption for all $t \in \mathbb{R}$, this is a positive multiple of \mathbf{e}_1 as required. Analogously, when $\ell = 1$ we have $|\tilde{f}(x) - \ell| = 1 - \sigma(g(x))$, and we therefore obtain a negative multiple of \mathbf{e}_1 and the result follows.

APPENDIX D. THE TWO HALF-BALLS MODEL

Let $n > 0$ be an integer indicating the dimension of the space from which data are sampled, let $\epsilon \geq 0$, and suppose that data are sampled from two classes with binary labels $\{0, 1\}$. Data of class 0 are sampled uniformly from the half-ball $D_0 = \{x \in \mathbb{R}^n : x + \epsilon \mathbf{e}_1 \in H^- \mathbb{B}^n\}$, where $\mathbf{e}_1 = (1, 0, \dots, 0)^\top \in \mathbb{R}$, while data from class 1 are sampled uniformly from the half-ball $D_1 = \{x \in \mathbb{R}^n : x - \epsilon \mathbf{e}_1 \in H^+ \mathbb{B}^n\}$. Here, we use the notation $H^- \mathbb{B}^n = \{x \in \mathbb{B}^n : x \cdot \mathbf{e}_1 < 0\}$ and $H^+ \mathbb{B}^n = \{x \in \mathbb{B}^n : x \cdot \mathbf{e}_1 > 0\}$. The two half-balls D_0, D_1 from which data points are sampled are separated by a margin of 2ϵ , and any pair of data points x, y sampled with opposite classes therefore satisfy $\|x - y\| \geq 2\epsilon$. We denote the combined distribution by $\mathcal{D}_\epsilon = \mathcal{U}(D_0 \cup D_1)$.

A classification function which produces the correct labels for this data can be defined by

$$f(x) = \begin{cases} 0 & \text{if } x_1 < 0, \\ 1 & \text{otherwise.} \end{cases}$$

Data points sampled from both classes are separated from the decision surface of this classifier by distance at least ϵ . On the other hand, for any $\delta > \epsilon$, there are clearly points, sampled from near the boundary of each class such that there exist destabilising perturbations $s \in \mathbb{R}^n$ with $\|s\| \leq \delta$ and $f(x + s) \neq f(x)$. Moreover, in high dimensions, data points sampled from such a distribution concentrate close to this decision surface, meaning that the probability of sampling a point which is susceptible to an adversarial attack is high, as encapsulated in the following result.

Theorem 10 (Susceptible data points are typical). *Let $\delta > \epsilon > 0$. Then,*

$$\begin{aligned} & P(x \sim \mathcal{D}_\epsilon : \text{there exists } s \in \mathbb{R}^n \\ & \quad \text{with } \|s\| \leq \delta \text{ such that } f(x + s) \neq f(x)) \\ & \geq 1 - (1 - (\delta - \epsilon)^2)^{n/2}. \end{aligned}$$

Although this susceptibility may be viewed as typical in high dimensions, however, the probability of detecting it by sampling random perturbations of data points is paradoxically very unlikely when $\epsilon > 0$, as shown by the following result.

Theorem 11 (Destabilising perturbations are rare). *Let $\delta > \epsilon > 0$. Then,*

$$\begin{aligned} P(x \sim \mathcal{D}_\epsilon, s \sim \mathcal{U}(\mathbb{B}_\delta^n) : f(x+s) \neq f(x)) \\ \leq \frac{1}{4} \left(1 - \left(\frac{\epsilon}{\delta}\right)^2\right)^{n/2}. \end{aligned}$$

D.1. Proof of Theorem 10. Using the definition of the classification function f , we may rewrite the probability in question as

$$\begin{aligned} P(x \sim \mathcal{D}_\epsilon : \text{there exists } s \in \mathbb{R}^n \text{ with } \|s\| \leq \delta \\ \text{such that } f(x+s) \neq f(x)) = P(x \sim \mathcal{D}_\epsilon : |x_1| < \delta). \end{aligned}$$

Expanding the probability as an integral, and using the fact that \mathcal{D}_ϵ is a uniform distribution over two disjoint half-balls and therefore has density $(V^n)^{-1}$, we may further express this as

$$\begin{aligned} P(x \sim \mathcal{D}_\epsilon : |x_1| < \delta) = \frac{1}{V^n} \left(\int_{D_0} \mathbb{I}_{\{x : -\delta < x_1 < -\epsilon\}} dx \right. \\ \left. + \int_{D_1} \mathbb{I}_{\{x : \epsilon < x_1 < \delta\}} dx \right), \end{aligned}$$

and the remaining problem is to compute the two remaining integrals, the values of which are equal by symmetry. We may express the set $\{x \in D_1 : \epsilon < x_1 < \delta\}$, which geometrically represents the slab of the half-ball D_1 within $\delta - \epsilon$ distance of its planar face, as the complement of a spherical cap, implying

$$\int_{D_1} \mathbb{I}_{\{x : \epsilon < x_1 < \delta\}} dx = \frac{1}{2} V^n - V_{\text{cap}}^n(1, 1 - (\delta - \epsilon)),$$

and therefore

$$P(x \sim \mathcal{D}_\epsilon : |x_1| < \delta) = 1 - \frac{2V_{\text{cap}}^n(1, 1 - (\delta - \epsilon))}{V^n}.$$

We may further estimate this from below, to show the exponential behaviour of this quantity with respect to n , by enveloping the spherical cap within a small half-ball. The Pythagorean theorem implies that

$$\{x \in D_1 : \epsilon < x_1 < \delta\} \subset G$$

where

$$G = \{x \in \mathbb{R}^n : x_1 > \epsilon \text{ and } \|x - \epsilon \mathbf{e}_1\|^2 \leq 1 - (\delta - \epsilon)^2\},$$

and therefore

$$\frac{2V_{\text{cap}}^n(1, 1 - (\delta - \epsilon))}{V^n} \leq (1 - (\delta - \epsilon)^2)^{n/2},$$

which proves the theorem.

D.2. Proof of Theorem 11. Since D_0 and D_1 are disjoint half-balls of a unit ball, it follows that the density associated with \mathcal{D}_ϵ is simply $(V^n)^{-1}$, while the density associated with $\mathcal{U}(\mathbb{B}_\delta^n)$ is $(\delta^n V^n)^{-1}$. Writing the probability as an integral with this density, we therefore find that

$$\begin{aligned} P(x \sim \mathcal{D}_\epsilon, s \sim \mathcal{U}(\mathbb{B}_\delta^n) : f(x+s) \neq f(x)) \\ = \frac{1}{\delta^n (V^n)^2} \left(\int_{D_0} \int_{\mathbb{B}_\delta^n} \mathbb{I}_{\{x, s : s_1 > -x_1\}} ds dx \right. \\ \left. + \int_{D_1} \int_{\mathbb{B}_\delta^n} \mathbb{I}_{\{x, s : s_1 < -x_1\}} ds dx \right). \end{aligned}$$

Probability of sampling a point and a perturbation s.t. the perturbation changes the class of the point, with data margin $\epsilon = 0.01$

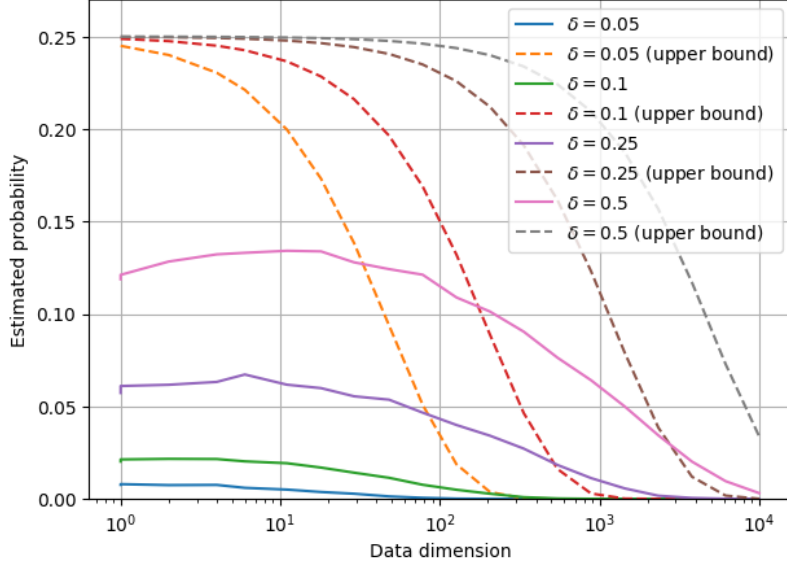


FIGURE 18. Comparing the upper bound from Theorem 11 against empirically computed probabilities for data sampled from uniform distributions in two half-balls with offset ϵ , and perturbations sampled uniformly from a ball with radius delta. We see that, even for comparatively large perturbations (e.g. $\delta = 0.5$, $\epsilon = 0.01$), the probability of randomly sampling a perturbation which changes the classification of a random data point is very small.

Since the values of these two integrals are equal by symmetry, we proceed by only estimating the first. For $x \in D_0$, we have $x_1 < -\epsilon$, and therefore

$$\begin{aligned} \int_{D_0} \int_{\mathcal{B}_\delta^n} \mathbb{I}_{\{x, s: s_1 > -x_1\}} ds dx &\leq \int_{D_0} dx \int_{\mathcal{B}_\delta^n} \mathbb{I}_{\{s: s_1 > \epsilon\}} ds \\ &= \frac{1}{2} V^n \int_{\mathcal{B}_\delta^n} \mathbb{I}_{\{s: s_1 > \epsilon\}} ds. \end{aligned}$$

The remaining integral over s now takes the form of the volume of a spherical cap, which we may bound by enveloping the cap in a small half-ball. Arguing as in the proof of Theorem 10, it follows that

$$\begin{aligned} \int_{\mathcal{B}_\delta^n} \mathbb{I}_{\{s: s_1 > \epsilon\}} ds &= V_{\text{cap}}^n(\delta, (\delta^2 - \epsilon^2)^{1/2}) \\ &\leq \frac{1}{2} \delta^n V^n \left(1 - \left(\frac{\epsilon}{\delta}\right)^2\right)^{n/2}. \end{aligned}$$

The result therefore follows by combining the components above.

APPENDIX E. GENERALISING THE THEORETICAL MODEL

We now show that the simple case presented in Section 3 extends to the more general cases demonstrated in Figure 4, in which the classification surface is not assumed to be flat, and the data are sampled from more general distributions. To demonstrate that these abstract results are true generalisations of the results show in Section 3, we derive corollaries to each result for a general SmAC distribution with a flat decision surface. These corollaries are therefore directly comparable with the results in Section 3 for specific indicated values of the parameters.

Let $\nu, w \in \mathbb{R}^n$ with $\|\nu\| = 1$, and define the plane

$$\pi = \{x \in \mathbb{R}^n : (x - w) \cdot \nu = 0\} \subset \mathbb{R}^n,$$

which passes through w and is normal to the vector ν . Denote by $\Pi : \mathbb{R}^n \rightarrow \pi$ the orthogonal projection operator onto π in the Euclidean inner product, given by

$$\Pi x = x - ((x - w) \cdot \nu)\nu.$$

Let $\phi : \pi \rightarrow \mathbb{R}$ be continuous, and define the surface

$$S = \{x \in \mathbb{R}^n : x - \phi(\Pi x)\nu \in \pi\} \subset \mathbb{R}^n.$$

A projector $\Gamma : \mathbb{R}^n \rightarrow S$ onto the surface S (along the vector ν) can be defined by

$$\Gamma x = \Pi x + \phi(\Pi x)\nu.$$

Remark 12 (Generalisation to other decision surfaces). *This can be generalised to incorporate other ‘wiggly’ decision surfaces. For instance, if S cannot be expressed as a modification of a hyperplane in its normal direction, one could instead consider the surfaces defined by the upper and lower graphs of S with respect to π , i.e. if S is given by a multi-valued function, one could instead just take the maximum or minimum values, and where necessary work with a Lipschitz extension of these surfaces. Our results below will extend to this case, albeit with some additional looseness reflecting the ‘uncertainty’ this imposes on the location of the decision surface of the classifier. Alternatively, the constructions above may be applied piecewise locally, splitting the surface S up into regions where the model adopted here can be applied directly. We do not strive for such generality here, though, in order to present the main ideas in a simple framework.*

We also introduce the signed directed distance functions $d_\pi : \mathbb{R}^n \rightarrow \mathbb{R}$ measuring the signed distance from a point x to the plane π along the normal vector ν , given by

$$d_\pi(x) = (x - \Pi x) \cdot \nu = (x - w) \cdot \nu,$$

and $d_S : \mathbb{R}^n \rightarrow \mathbb{R}$ measuring the signed distance from a point x to the surface S along the vector ν , given by

$$\begin{aligned} d_S(x) &= (x - \Gamma(x)) \cdot \nu = (x - \Pi x) \cdot \nu - \phi(\Pi x) \\ &= d_\pi(x) - \phi(\Pi x). \end{aligned}$$

Finally, we can define the distance from a point x to the surface S by

$$\sigma(x) = \inf_{\hat{y} \in S} \|x - \hat{y}\|,$$

noting the trivial inequality

$$(6) \quad \sigma(x) \leq |d_S(x)|,$$

for any $x \in \mathbb{R}^n$, since d_S only measures distance to S in the direction of ν while σ measures the shortest distance to S over all directions.

With these constructions, we can define a binary classifier with decision surface S as the function $f : \mathbb{R}^n \rightarrow \{0, 1\}$ given by

$$f(x) = \begin{cases} 0 & \text{if } d_S(x) \leq 0, \\ 1 & \text{otherwise.} \end{cases}$$

To show how our previous results extend into this more general case, suppose that data points of class 0 are sampled from a distribution \mathcal{D} on \mathbb{R}^n , and that data points of class 1 are sampled from the distribution \mathcal{D}' on \mathbb{R}^n . In the interests of simplicity, we only study the behaviour of the classifier on the class 0, as the result for the class 1 is, in some sense, symmetric. We study this more general model in parallel with the results of Section 3.

We first observe that the accuracy of the classifier may be controlled in an analogous way to the simple case in Section 3. The supremum in this result (and the suprema and infima in subsequent results) is simply present to ensure an optimal balancing for the two terms; a valid (though possibly sub-optimal) result may be obtained by selecting any value of $\alpha \geq 0$. The first

term appearing on the right hand side controls how far the surface S may be expected to deviate from the plane π (and is therefore simply 1 in the case when $\phi \equiv 0$ and so $S = \pi$; in this case the optimal balancing of the terms will be obtained when $\alpha = 0$). The second term, on the other hand, estimates the probability that a point is correctly classified by the plane placed parallel to π , but offset by distance α to account for the variability of ϕ . If the distribution \mathcal{D} is just the uniform distribution in a ball with centre at distance $\epsilon < 0$ from the plane π , therefore, this recovers the result of Theorem 2 for a single class.

Theorem 13 (Accuracy of the classifier f). *Suppose that a point x is sampled with class 0. Then, the probability that the classifier f correctly classifies x is at least*

$$\begin{aligned} P(x \sim \mathcal{D} : f(x) = 0) \\ \geq \sup_{\alpha \geq 0} [P(x \sim \mathcal{D} : |\phi(\Pi x)| \leq \alpha) \\ - P(x \sim \mathcal{D} : d_\pi(x) > -\alpha)]. \end{aligned}$$

We demonstrate this result in the setting of a linear classifier with a distribution \mathcal{E} which satisfies the SmAC condition of Definition 1 with radius $r > 0$ and centre c such that $d_\pi(c) = -\eta$ for some $\eta \in [0, r)$. Then, Theorem 13 takes the following form, from which we obtain Theorem 2 when $r = 1$ and $\eta = \epsilon$.

Corollary 14 (Accuracy for SmAC distributions). *Suppose that points with label 0 are sampled from the distribution \mathcal{E} , and suppose that $\phi \equiv 0$. Then, the probability that the classifier f accurately classifies points of class 0 is at least*

$$P(x \sim \mathcal{E} : f(x) = 0) \geq 1 - \frac{1}{2} A^n \left(1 - \left(\frac{\eta}{r}\right)^2\right)^{\frac{n}{2}}.$$

We may also prove the susceptibility result of Theorem 3 in our abstract setting. The probability of sampling a data point which is susceptible to an adversarial attack of size δ may be bounded from below as in the following result. The form of this result is similar to that of Theorem 13, although we note the crucial difference in the second term.

Theorem 15 (Susceptibility to adversarial perturbations). *Suppose that points with label 0 are sampled from the distribution \mathcal{D} . Then, for any $\delta > 0$, the probability that a point sampled at random from the class 0 is susceptible to an adversarial attack with Euclidean norm δ is at least*

$$\begin{aligned} P(x \sim \mathcal{D} : \text{there exists } s \in \mathbb{B}_\delta^n \text{ with } f(x + s) \neq 0) \\ \geq \sup_{\alpha \geq 0} [P(x \sim \mathcal{D} : |\phi(\Pi x)| \leq \alpha) \\ - P(x \sim \mathcal{D} : d_\pi(x) \leq \alpha - \delta)]. \end{aligned}$$

When applied to the SmAC distribution \mathcal{E} , this result takes the following form, from which we obtain Theorem 3.

Corollary 16 (Susceptibility for SmAC distributions). *Suppose that points with label 0 are sampled from the distribution \mathcal{E} , and suppose that $\phi \equiv 0$. Then, for any $\delta \in [\eta, r]$, the probability that a point sampled at random from the class 0 is susceptible to an adversarial attack with Euclidean norm δ is at least*

$$\begin{aligned} P(x \sim \mathcal{E} : \text{there exists } s \in \mathbb{B}_\delta^n \text{ with } f(x + s) \neq 0) \\ \geq 1 - \frac{1}{2} A^n \left(1 - \left(\frac{\delta - \eta}{r}\right)^2\right)^{\frac{n}{2}}. \end{aligned}$$

We also show a generalised version of Theorem 4, which bounds the probability of sampling a random perturbation which is adversarial for f . For this result, we assume that the surface S has some regularity, in the sense that the function ϕ is Lipschitz with constant $L > 0$; i.e. for any $\hat{x}, \hat{y} \in \pi$ we have $|\phi(\hat{x}) - \phi(\hat{y})| \leq L \|\hat{x} - \hat{y}\|$. Geometrically, this defines a cone of points around any $x \in \mathbb{R}^n$ in which f is guaranteed to be constant. This property is particularly useful to us here because it allows us to prove the following lower bound on σ by d_S in Section E.3.

Lemma 17 (Lipschitz regularity gives control of σ). *Suppose that ϕ is Lipschitz with parameter L . Then, for any $x \in \mathbb{R}^n$,*

$$(7) \quad \sigma(x) \geq |d_S(x)| \sin \theta,$$

where $\theta = \arctan(L^{-1})$.

This allows us to prove the following result, indicating that destabilising random perturbations may be expected to be rare.

Theorem 18 (Probability of sampling misclassifying random perturbations). *Suppose that points with label 0 are sampled from the distribution \mathcal{D} . Then, for any $\delta > 0$, the probability that a point sampled at random from the class 0 will be misclassified after the application of a perturbation randomly sampled uniformly from \mathbb{B}_δ^n is bounded by*

$$\begin{aligned} & P(x \sim \mathcal{D}, s \sim \mathbb{B}_\delta^n : f(x+s) \neq 0) \\ & \leq \inf_{\substack{\alpha, \gamma \geq 0 \\ t \in T(L)}} \left[P(x \sim \mathcal{D} : |\phi(\Pi x)| \geq \alpha) \right. \\ & \quad + P\left(x \sim \mathcal{D} : d_\pi(x) \geq -\alpha - \frac{t}{\sin \theta}\right) \\ & \quad + \Delta(L) \frac{1}{2} \left(1 - \left(\frac{t}{\delta} - L\right)^2\right)^{\frac{n}{2}} \\ & \quad \cdot \left(P(x \sim \mathcal{D} : d_\pi(x) \leq \gamma - t) \right. \\ & \quad \left. \left. + P(x \sim \mathcal{D} : |\phi(\Pi x)| > \gamma) \right) \right], \end{aligned}$$

where $\Delta(L) = 1$ for $L \leq 1$ and 0 for $L > 1$, and the set $T(L) = [\min\{L, 1\}\delta, \delta]$.

We also show this result for the SmAC distribution \mathcal{E} , from which Theorem 4 follows when $r = 1$ and $\eta = \epsilon$. In this case, we have $L = 0$ and so $\theta = \frac{\pi}{2}$ and therefore $\sin \theta = 1$, and the result of Theorem 18 produces the following corollary.

Corollary 19 (Destabilising random perturbations are rare for SmAC distributions). *Suppose that points with label 0 are sampled from the distribution \mathcal{E} , and suppose that $\phi \equiv 0$. Then, for any $\delta \in [\eta, r]$, the probability that a point sampled at random from the class 0 is misclassified after the application of a perturbation sampled uniformly from the ball \mathbb{B}_δ^n is bounded by*

$$P(x \sim \mathcal{E}, s \sim \mathbb{B}_\delta^n : f(x+s) \neq 0) \leq A^n \left(1 - \left(\frac{\eta}{r+\delta}\right)^2\right)^{\frac{n}{2}}.$$

E.1. Proof of Theorem 13 and Corollary 14.

E.1.1. *Proof of Theorem 13.* We can measure the accuracy of the classifier for class 0 as

$$\text{acc}_0(f) = P(x \sim \mathcal{D} : f(x) = 0) = P(x \sim \mathcal{D} : d_S(x) \leq 0).$$

For any $t \in \mathbb{R}$, the condition that $d_S(t) \leq t$ can be rewritten as

$$d_\pi(x) - \phi(\Pi x) \leq t,$$

which is implied by the condition that

$$d_\pi(x) + |\phi(\Pi x)| \leq t.$$

Introducing the event $A(\alpha)$, for any $\alpha \geq 0$, which occurs when a point $x \sim \mathcal{D}$ is such that $|\phi(\Pi x)| \leq \alpha$, and the event $B(\beta)$, for any $\beta \in \mathbb{R}$, which occurs when x is such that $d_\pi(x) \leq \beta$, we find that

$$(8) \quad A(\alpha) \wedge B(t - \alpha) \quad \Rightarrow \quad d_\pi(x) + |\phi(\Pi x)| \leq t.$$

Putting these pieces together, we find that

$$\begin{aligned} \text{acc}_0(f) & \geq P(x \sim \mathcal{D} : d_\pi(x) + |\phi(\Pi x)| \leq 0) \\ & \geq P(x \sim \mathcal{D} : A(\alpha) \wedge B(-\alpha)). \end{aligned}$$

Negating this event and applying the union bound, we therefore find that

$$\begin{aligned} \text{acc}_0(f) &\geq P(x \sim \mathcal{D} : |\phi(\Pi x)| \leq \alpha) \\ &\quad - P(x \sim \mathcal{D} : d_\pi(x) > -\alpha). \end{aligned}$$

Since $\alpha \geq 0$ was arbitrary, it therefore follows that

$$\begin{aligned} \text{acc}_0(f) &\geq \sup_{\alpha \geq 0} [P(x \sim \mathcal{D} : |\phi(\Pi x)| \leq \alpha) \\ &\quad - P(x \sim \mathcal{D} : d_\pi(x) > -\alpha)]. \end{aligned}$$

E.1.2. *Proof of Corollary 14.* Since $\phi \equiv 0$ in this case, it follows that

$$P(x \sim \mathcal{E} : |\phi(x)| \leq \alpha) = 1,$$

for all $\alpha \geq 0$. We may therefore take $\alpha = 0$ in the second term of Theorem 13, and we proceed by bounding

$$P(x \sim \mathcal{E} : d_\pi(x) \geq 0)$$

from above.

Recalling the bound on the density p of \mathcal{E} in Definition 1, we have

$$P(x \sim \mathcal{E} : d_\pi(x) \geq 0) \leq \frac{A^n}{V^{n_r n}} \int_{\mathbb{B}_r^n(c)} \mathbb{I}_{\{x : d_\pi(x) \geq 0\}} dx,$$

and the definition of d_π implies that this is

$$\int_{\mathbb{B}_r^n(c)} \mathbb{I}_{\{x : d_\pi(x) \geq 0\}} dx = \int_{\mathbb{B}_r^n(c)} \mathbb{I}_{\{x : (x-w) \cdot \nu \geq 0\}} dx,$$

which is zero for $(w-c) \cdot \nu > r$ and simply a spherical cap otherwise. Note that the assumption that $d_\pi(c) = -\eta$ for some $\eta > 0$ implies that this spherical cap is less than half the ball $\mathbb{B}_r^n(c)$. Therefore, Lemma 9 implies that

$$P(x \sim \mathcal{E} : f(x) = 0) \geq 1 - \frac{1}{2} A^n \left(1 - \left(\frac{\eta}{r}\right)^2\right)^{\frac{n}{2}}$$

E.2. Proof of Theorem 15 and Corollary 16.

E.2.1. *Proof of Theorem 15.* The susceptibility of points sampled from class 0 to an adversarial attack with Euclidean norm δ may be measured analogously using the function

$$\text{sus}_0(f) = P(x \sim \mathcal{D} : \text{there exists } s \in \mathbb{B}_\delta^n \text{ with } f(x+s) \neq 0).$$

The set of points x satisfying the condition in this probability may be seen to be those contained in the union $R \cup T$ of the disjoint sets

$$R = \{x \in \mathbb{R}^n : d_S(x) > 0\}$$

and

$$T = \{x \in \mathbb{R}^n : d_S(x) \leq 0 \text{ and } \sigma(x) \leq \delta\};$$

in the first case, since these points are already misclassified it follows that $f(x+s) \neq 0$ for $s = 0 \in \mathbb{B}_\delta^n$, while in the second case the points are correctly classified but they lie within Euclidean distance δ of the decision surface S , due to the definition of σ . To simplify this condition slightly, we observe that

$$\{x \in \mathbb{R}^n : d_S(x) \geq -\delta\} \subset R \cup T,$$

and therefore

$$\text{sus}_0(f) \geq P(x \sim \mathcal{D} : d_S(x) \geq -\delta)$$

Arguing as above, we have

$$d_S(x) = d_\pi(x) - \phi(\Pi x) \geq -\delta,$$

which is implied by the condition that

$$|\phi(\Pi x)| - d_\pi(x) \leq \delta.$$

Recalling the events $A(\alpha)$ and $B(\beta)$ from above, we see that for any $\alpha \geq 0$ this event is in turn implied by the event

$$A(\alpha) \wedge \text{not } B(\alpha - \delta),$$

from which it follows that

$$\text{sus}_0(f) \geq P(x \sim \mathcal{D} : A(\alpha) \wedge \text{not } B(\alpha - \delta)),$$

and negating this event and applying the union bound therefore implies that

$$\text{sus}_0(f) \geq P(x \sim \mathcal{D} : A(\alpha)) - P(x \sim \mathcal{D} : B(\alpha - \delta)),$$

and, since $\alpha \geq 0$ was arbitrary,

$$\begin{aligned} \text{sus}_0(f) &\geq \sup_{\alpha \geq 0} [P(x \sim \mathcal{D} : |\phi(\Pi x)| < \alpha) \\ &\quad - P(x \sim \mathcal{D} : d_\pi(x) < \alpha - \delta)]. \end{aligned}$$

E.2.2. Proof of Corollary 16. To prove the Corollary, we start from the result of Theorem 15. Setting $\phi \equiv 0$ and selecting $\alpha = 0$, we find that

$$\begin{aligned} P(x \sim \mathcal{E} : \text{there exists } s \in \mathbb{B}_\delta^n \text{ with } f(x + s) \neq 0) \\ \geq 1 - P(x \sim \mathcal{E} : d_\pi(x) < -\delta). \end{aligned}$$

To prove the result, we therefore bound this final term on the right from above.

Recalling the bound on the density p of \mathcal{E} in Definition 1, we have

$$P(x \sim \mathcal{E} : d_\pi(x) < -\delta) \leq \frac{A^n}{V^n r^n} \int_{\mathbb{B}_r^n(c)} \mathbb{I}_{\{x : d_\pi(x) < -\delta\}} dx.$$

Here, the assumption that $\delta \in (\eta, r]$ implies that this integral is over a spherical cap which is smaller than a hemisphere, and so we conclude that

$$P(x \sim \mathcal{E} : d_\pi(x) < -\delta) \leq \frac{1}{2} A^n \left(1 - \left(\frac{\delta - \eta}{r}\right)^2\right)^{\frac{n}{2}},$$

and the result follows.

E.3. Proof of Lemma 17, Theorem 18 and Corollary 19.

E.3.1. Proof of Lemma 17. Geometrically, for any point $x \in \mathbb{R}^n$, the Lipschitz condition of ϕ defines a cone $C(x)$ of points y such that $y \in C(x)$ implies that $d_S(y) \leq 0$, where

$$C(x) = \{y \in \mathbb{R}^n : (y - \Gamma(x)) \cdot \nu \leq m \|y - \Gamma(x)\|\},$$

with $m = -\cos \theta$ and $\theta = \arctan(L^{-1})$.

Suppose that $z \in \mathbb{R}^n$ is a point which f classifies as class 0, i.e. such that $d_S(z) \leq 0$. The Lipschitz condition on ϕ provides a cone of points $C(z)$ around z which are guaranteed to also have class 0. This allows us to use a geometric argument to find a lower bound on σ in terms of d_S . Placing a ball $\mathbb{B}_\epsilon^n(z)$ of radius ϵ around z for some $\epsilon \geq 0$, we can observe that the cone $C(z)$ is tangent to this ball when $\epsilon = |d_S(z)| \sin \theta$. This is due to the fact that z lies on the central axis of $C(z)$ (which is oriented in the direction of ν) and $|d_S(z)|$ therefore measures the distance from z to the vertex of $C(z)$. This therefore implies the lower bound that

$$\sigma(z) \geq |d_S(z)| \sin \theta,$$

which we may view as the companion to the upper bound (6). This allows us to control σ from below using d_S , which would not have been possible without such a regularity condition on the surface S .

E.3.2. *Proof of Theorem 18.* Define the probability of randomly sampling an adversarial perturbation as

$$\text{rand}_0(f) = P(x \sim \mathcal{D}, s \sim \mathcal{U}(\mathbb{B}_\delta^n) : f(x+s) \neq 0),$$

for some fixed $\delta > 0$. Clearly this condition will only hold for a point x if x is either already misclassified by f or such that $\sigma(x) < \delta$, and therefore we have

$$\begin{aligned} \text{rand}_0(f) &= P(x \sim \mathcal{D}, s \sim \mathcal{U}(\mathbb{B}_\delta^n) : f(x) \neq 0 \\ &\quad \text{or } (\sigma(x) \leq \delta \text{ and } f(x+s) \neq 0)). \end{aligned}$$

Recalling the definition of d_S , we can express this as

$$\begin{aligned} \text{rand}_0(f) &= P(x \sim \mathcal{D}, s \sim \mathcal{U}(\mathbb{B}_\delta^n) : d_S(x) > 0 \\ &\quad \text{or } (\sigma(x) \leq \delta \text{ and } f(x+s) \neq 0)). \end{aligned}$$

To obtain a bound which generalises Theorem 4, we slightly refine this by splitting the probability into two parts. Let $t \in [0, \delta]$ and introduce the sets

$$K = \{x \in \mathbb{R}^n : d_S(x) > 0 \text{ or } \sigma(x) \leq t\},$$

which contains those points which are misclassified by f alongside those points which are correctly classified but distance t from the decision boundary, and

$$U = \{x \in \mathbb{R}^n : d_S(x) < 0 \text{ and } \sigma(x) \in (t, \delta]\},$$

which contains the correctly classified points which are distance t to δ from the decision boundary. Since these two sets are disjoint, we therefore have

$$\begin{aligned} (9) \quad \text{rand}_0(f) &= P(x \sim \mathcal{D}, s \sim \mathcal{U}(\mathbb{B}_\delta^n) : x \in K \text{ and } f(x+s) \neq 0) \\ &\quad + P(x \sim \mathcal{D}, s \sim \mathcal{U}(\mathbb{B}_\delta^n) : x \in U \text{ and } f(x+s) \neq 0), \end{aligned}$$

and we obtain bounds on these two terms separately. Analogously to the proof of Theorem 4, the philosophy here is that the first term is ‘small’ since it only contains those points which are misclassified by a slightly worse classifier, while the second term is small because only a small fraction of the sampled perturbations $s \in \mathbb{B}_\delta^n$ are sufficiently large to push the points across the decision boundary.

To bound the first term of (9), we use the lower bound of Lemma 17 on σ in terms of d_S to show that the condition $\sigma(x) \leq t$ implies that $|d_S(x)| \leq \frac{t}{\sin \theta}$. From this, the set inclusion

$$K \subset V = \left\{ x \in \mathbb{R}^n : d_S(x) \geq -\frac{t}{\sin \theta} \right\}$$

follows, enabling us to simplify the term to be bounded as

$$\begin{aligned} &P(x \sim \mathcal{D}, s \sim \mathcal{U}(\mathbb{B}_\delta^n) : x \in K \text{ and } f(x+s) \neq 0) \\ &\leq P(x \sim \mathcal{D} : x \in K) \leq P(x \sim \mathcal{D} : x \in V). \end{aligned}$$

Recalling the definition of the events $A(\alpha)$ and $B(\beta)$ introduced above, for any $\alpha \geq 0$ the event $A(\alpha) \wedge B(-\alpha - \frac{t}{\sin \theta})$ implies that the event $x \notin V$ holds, and therefore

$$\begin{aligned} P(x \sim \mathcal{D} : x \in V) &= 1 - P(x \sim \mathcal{D} : x \notin V) \\ &\leq 1 - P\left(A(\alpha) \wedge B\left(-\alpha - \frac{t}{\sin \theta}\right)\right). \end{aligned}$$

Inverting this final probability, the union bound therefore implies that

$$\begin{aligned} P(x \sim \mathcal{D} : x \in V) &\leq P(\text{not } A(\alpha)) \\ &\quad + P\left(\text{not } B\left(-\alpha - \frac{t}{\sin \theta}\right)\right), \end{aligned}$$

and therefore, since $\alpha \geq 0$ was arbitrary,

$$(10) \quad \begin{aligned} P(x \sim \mathcal{D} : x \in V) \\ \leq \inf_{\alpha \geq 0} \left(P(x \sim \mathcal{D} : |\phi(\Pi x)| \geq \alpha) \right. \\ \left. + P\left(x \sim \mathcal{D} : d_\pi(x) \geq -\alpha - \frac{t}{\sin \theta}\right) \right), \end{aligned}$$

for any $t \in [0, \delta]$, which completes our bound on the first term of (9).

Turning to the second term of (9), we can simplify things by including the set U into the larger set

$$U \subset G = \{x \in \mathbb{R}^n : d_S(x) < -t\},$$

where the inclusion holds due to the upper bound (6) on σ . The reason for this inclusion is that it allows us to study the intersection of the cone $C(x)$ of points with the same classification as x (the existence of which is ensured by the Lipschitz property on ϕ) with the ball of perturbed data points $\mathbb{B}_\delta^n(x)$. Specifically, for any $x \in G$, define set

$$H(x) = \mathbb{B}_\delta^n(x) \setminus (\mathbb{B}_\delta^n(x) \cap C(x))$$

of perturbations of x which are taken outside the cone $C(x)$ of points guaranteed to be correctly classified.

Suppose that $L > 1$. Then, for $t > \delta L$ the set $H(x)$ may be included in a spherical cap which forms less than a hemisphere of $\mathbb{B}_\delta^n(x)$, and which may itself be contained in the larger spherical cap

$$H(x) \subset \{y \in \mathbb{B}_\delta^n(x) : (y - x) \cdot \nu > |d_S(x)| - \delta L\}.$$

Since $x \in G$ implies that $d_S(x) < -t$, it therefore follows that

$$H(x) \subset J(x) = \{y \in \mathbb{B}_\delta^n(x) : (y - x) \cdot \nu > t - \delta L\},$$

and Lemma 9 implies that the volume of $J(x)$ may be bounded by

$$\frac{1}{2} V^n \delta^n \left(1 - \left(\frac{t}{\delta} - L\right)^2\right)^{\frac{n}{2}}$$

Consequently, since perturbations are sampled uniformly from \mathbb{B}_δ^n , we obtain the bound

$$\begin{aligned} P(x \sim \mathcal{D}, s \sim \mathcal{U}(\mathbb{B}_\delta^n) : x \in U \text{ and } f(x + s) \neq 0) \\ \leq \frac{1}{2} \left(1 - \left(\frac{t}{\delta} - L\right)^2\right)^{\frac{n}{2}} P(x \sim \mathcal{D} : x \in G). \end{aligned}$$

To compute the probability of sampling $x \in G$, we recall the definition of the events $A(\alpha)$ and $B(\beta)$ introduced above, and observe that for any $\gamma \geq 0$

$$A(\gamma) \wedge \text{not } B(\gamma - t) \quad \Rightarrow \quad d_S(x) > -t,$$

and therefore, since

$$\begin{aligned} P(x \sim \mathcal{D} : x \in G) &= 1 - P(x \sim \mathcal{D} : d_S(x) > -t) \\ &\leq 1 - P(x \sim \mathcal{D} : A(\gamma) \wedge \text{not } B(\gamma - t)), \end{aligned}$$

it follows from negating this event, applying the union bound, and recalling that $\gamma \geq 0$ was arbitrary, that

$$(11) \quad P(x \sim \mathcal{D} : x \in G) \\ (12) \quad \leq \inf_{\gamma \geq 0} [P(x \sim \mathcal{D} : d_\pi(x) \leq \gamma - t) \\ (13) \quad + P(x \sim \mathcal{D} : |\phi(\Pi x)| > \gamma)].$$

For $L > 1$, however, it is not possible to take $t > \delta L$ since $t \in [0, \delta]$ and so selecting $t = \delta$ provides an optimal result here. In this case, the set U is empty, so this term is simply zero.

Combining the bounds (10) and (11), we therefore find that

$$\begin{aligned} & \text{rand}_0(f) \\ & \leq \inf_{\substack{\alpha, \gamma \geq 0 \\ t \in T(L)}} \left[P(x \sim \mathcal{D} : |\phi(\Pi x)| \geq \alpha) \right. \\ & \quad + P\left(x \sim \mathcal{D} : d_\pi(x) \geq -\alpha - \frac{t}{\sin \theta}\right) \\ & \quad + \Delta(L) \frac{1}{2} \left(1 - \left(\frac{t}{\delta} - L\right)^2\right)^{\frac{n}{2}} \\ & \quad \cdot (P(x \sim \mathcal{D} : d_\pi(x) \leq \gamma - t) \\ & \quad \left. + P(x \sim \mathcal{D} : |\phi(\Pi x)| > \gamma)) \right], \end{aligned}$$

where $\Delta(L) = 1$ for $L \leq 1$ and 0 for $L > 1$, and the set $T(L) = [\min\{L, 1\}\delta, \delta]$.

E.3.3. *Proof of Corollary 19.* Since $\phi \equiv 0$, it follows that $L = 0$ and therefore $\theta = 0$. Applying these facts to the result of Theorem 18, and selecting $\alpha = \gamma = 0$, we immediately find that

$$(14) \quad \begin{aligned} & P(x \sim \mathcal{E}, s \sim \mathbb{B}_\delta^n : f(x+s) \neq 0) \\ & \leq \inf_{t \in [0, \delta]} \left[P(x \sim \mathcal{E} : d_\pi(x) \geq -t) \right. \\ & \quad \left. + \frac{1}{2} \left(1 - \left(\frac{t}{\delta}\right)^2\right)^{\frac{n}{2}} (P(x \sim \mathcal{E} : d_\pi(x) \leq -t)) \right]. \end{aligned}$$

Using the crude bound

$$P(x \sim \mathcal{E} : d_\pi(x) \geq -t) \leq 1,$$

this may be simplified to

$$\begin{aligned} & P(x \sim \mathcal{E}, s \sim \mathbb{B}_\delta^n : f(x+s) \neq 0) \\ & \leq \inf_{t \in [0, \delta]} \left[P(x \sim \mathcal{E} : d_\pi(x) \geq -t) + \frac{1}{2} \left(1 - \left(\frac{t}{\delta}\right)^2\right)^{\frac{n}{2}} \right]. \end{aligned}$$

Recalling the bound on the density p of \mathcal{E} in Definition 1, we have

$$P(x \sim \mathcal{E} : d_\pi(x) \geq -t) \leq \frac{A^n}{V^n r^n} \int_{\mathbb{B}_r^n(c)} \mathbb{I}_{\{x : d_\pi(x) \geq -t\}} dx,$$

and, arguing as in the proof of Corollary 14, we note that this may be bounded by

$$P(x \sim \mathcal{E} : d_\pi(x) \geq -t) \leq \frac{1}{2} A^n \left(1 - \left(\frac{\eta - t}{r}\right)^2\right)^{\frac{n}{2}}$$

for any $t \in [0, \delta]$. Substituting this bound into (14) and selecting $t = \frac{\eta\delta}{r+\delta}$ (which is a valid choice of t because $\frac{\eta\delta}{r+\delta} \in [0, \frac{\eta}{r+1}]$ for $\delta \in [0, 1]$ and $\eta \in [0, r)$) produces the result.